

# Mass-Transfer Coefficients in Washcoated Monoliths

Madhuchhanda Bhattacharya, Michael P. Harold, and Vemuri Balakotaiah

Dept. of Chemical Engineering, University of Houston, Houston, TX 77204

DOI 10.1002/aic.10212

Published online in Wiley InterScience (www.interscience.wiley.com).

*The asymptotic mass-transfer coefficients are determined in washcoated monoliths of various geometric shapes by solving the convection–diffusion equation in the fluid phase coupled with the diffusion–reaction equation in the washcoat. The dependency of the asymptotic Sherwood number ( $Sh_\infty$ ) on washcoat properties (relative effective washcoat thickness  $\lambda$ , ratio of diffusivity of reactant in the fluid phase to that in the washcoat  $\delta$ , and the catalyst loading  $\phi_s^2$ ) is examined. It is found that in the kinetic regime ( $\phi_s^2 \rightarrow 0$ ),  $Sh_\infty$  approaches a new asymptote ( $Sh_{w,\infty}$ ) which depends on the flow as well as washcoat geometries. For  $\delta \rightarrow 0$ ,  $Sh_{w,\infty}$  approaches  $Sh_{H_1,\infty}$  corresponding to flow geometry, whereas for  $\delta \rightarrow \infty$  it approaches  $Sh_{H_2,\infty}$  of flow geometry. As can be expected, in the mass transfer controlled regime,  $Sh_\infty$  approaches  $Sh_{T,\infty}$  (flow geometry), which is independent of washcoat properties. It is also found that the variation of  $Sh_\infty$  with catalyst loading is not always monotonic when washcoat distribution around the channel perimeter is nonuniform. Numerical results, describing the variation of  $Sh_\infty$  with washcoat properties, are presented for some commonly used channel geometries. © 2004 American Institute of Chemical Engineers *AIChE J*, 50: 2939–2955, 2004*

**Keywords:** catalytic monolith, washcoat diffusion, asymptotic mass transfer coefficients, convection–diffusion–reaction equation, Sherwood number

## Introduction

Monolith catalysts were first developed in the 1970s for automotive exhaust gas treatment, mainly to control the hydrocarbon and carbon monoxide emissions. Over the last 20–30 years, these reactors have been used primarily as air pollution control devices because of their unique characteristics of low pressure drop, high specific external surface area, and less catalyst attrition compared to those of the packed-bed reactors. One recent application of monolith reactors is the selective catalytic reduction (SCR) of  $\text{NO}_x$  released from stationary or mobile sources (Forzatti, 2001), where low pressure drop is of great advantage. Other potential applications of monolith reactors include, but are not restricted to, catalytic partial oxida-

tions, gas turbines used in power generation, and liquid-phase hydrogenations (Cybulski and Moulijn, 1994).

Monolithic reactors consist of a matrix of uniformly aligned parallel channels of roughly 1–2 mm inside dimension, fabricated on either ceramic or metallic supports. These supports, also known as substrates, are available in a variety of cross-sectional shapes including circles, squares, hexagons, triangles, and sinusoids. In most applications, the reacting fluid flows through these channels in laminar flow regime (Reynolds number between 10 to 1000) with fully developed flow in the greatest part of the reactor (Bennett et al., 1992; Young and Finlayson, 1976), where reactants are transported to the substrate mainly by molecular diffusion. The substrate wall is treated with a 10- to 200- $\mu\text{m}$ -thick porous layer containing catalyst supports, stabilizers, and promoters, commonly called as *washcoat*, where the active metal sites are dispersed by impregnation. Within the washcoat, the reactants diffuse and react on the active catalyst sites with an associated release or absorption of heat.

Correspondence concerning this article should be addressed to V. Balakotaiah at bala@uh.edu.

The presence of catalytic reactions at the wall of the channel acts as a source or sink and imposes concentration or temperature gradients in the transverse directions, which are normal to the flow direction where the reactants are mainly transported by convection. The extent of transverse variations depends mainly on the relative rate of the mass or heat transfer across the channel compared to that of the catalytic reactions. At low operating temperatures, higher transfer rates lead to a nearly uniform concentration or temperature distribution within the channel. In the literature, this regime is called *kinetically controlled*, where the overall reactor performance is limited by the slow reaction rates. A sharper increase of the reaction rates with temperature, following the Arrhenius law, circumvents the mass- or heat-transfer process at higher temperatures and the reactor operation is reversed to the mass transfer controlled regime. In this regime, the mass transfer across the channel restricts the reactant conversion, creating strong gradients in the transverse directions. Many models have been proposed in the literature to describe this intricate coupling between the mass- or heat-transfer and the chemical reaction starting from lumped parameter models (Oh and Cavendish, 1983; Tronconi and Forzatti, 1992) to distributed models (see, for example, Lee and Aris, 1977; Young and Finlayson, 1976) with a varying degree of complexity. These models revolved around the derivation of the simplest one that can illustrate the mass or heat transfer within the channel retaining all the qualitative features of the washcoated catalyst (Heck et al., 1976; Hegedus, 1975).

A major simplification, which has been followed historically in monolith literature, is to represent the whole matrix by a single channel with the assumption of equivalent passages with no interaction. As mentioned earlier, the mass or heat transfer within a single channel can be described by two inherently coupled processes: external transfer from the bulk to the substrate and internal transfer inside the porous washcoat. Hence, the steady-state behavior of a single channel can be mathematically described by a convection–diffusion equation in the fluid phase coupled with the diffusion–reaction equation within the washcoat involving more than one spatial dimension. Instead, the monoliths have been studied by decoupling the above two processes while lumping the effect of washcoat diffusion into the well-known effectiveness factor (Aris, 1975; Leung et al., 1996; Papadias et al., 2000). This resulted in two broadly classified hierarchical models: two-dimensional (2-D) convection–diffusion model with wall reaction (Balakotaiah et al., 2000; Damköhler, 1937; Hayes et al., 1992; Lee and Aris, 1977) and 1-D two-phase model (Ablow and Wise, 1979; Bensalem and Ernst, 1982). Over the years, the 1-D two-phase models, which are derived by averaging the full model over the channel cross section, have become more popular because of their simplicity and ease of computation.

In the two-phase model, the transfer across the channel is related to the difference between the cup-mixing and wall concentrations (or temperatures) by introducing an effective mass- (or heat-) transfer coefficient, whereas the effectiveness factor captures the diffusion and reaction within the washcoat. The transfer coefficients that appear in the two-phase model depend on various system parameters (such as shape and dimensions of the channel, kinetic parameters, fluid and washcoat properties, and so on) and are often expressed in dimensionless form as Sherwood (Sh) and Nusselt (Nu) numbers. In the chemical engineering literature, it is a common practice to

use a constant value for the Sh or Nu, which corresponds to the asymptotic value reached in long channels. These asymptotic values for various channel geometries and operating regimes can be calculated from the solutions of the two- or three-dimensional problems (Shah and London, 1978).

In this work, we present a comprehensive analysis for long and narrow channels, where the entry effect is negligible, and determine the asymptotic Sherwood numbers,  $Sh_\infty$ , in the presence of washcoat diffusion by solving the coupled convection–diffusion–reaction equations in a single channel. More specifically, we present the asymptotic Sherwood numbers for channels of various geometric shapes with or without sharp corners and determine the influence of washcoat properties on  $Sh_\infty$ . In the heat-transfer literature, the asymptotic Nu numbers for straight ducts with wall heat transfer have been classified broadly in eight categories, depending on the imposed boundary conditions (Shah and London, 1978). Among them, only three are of interest to chemical engineers: (1) constant temperature asymptote  $Nu_{T,\infty}$ , where both circumferentially and axially uniform wall temperature is specified; (2) constant flux asymptote of the first kind,  $Nu_{H_1,\infty}$ , where circumferentially constant wall temperature and axially constant wall flux are specified; and (3) constant flux asymptote of the second kind,  $Nu_{H_2,\infty}$ , where both axially and circumferentially uniform wall fluxes are specified. It is a well known fact that, for a straight circular channel with wall reactions, the asymptotic Sherwood numbers are bounded by constant flux and constant concentration (temperature) asymptotes and vary smoothly from one to the other as the local Damköhler number  $\phi_s^2$  varies from 0 to  $\infty$  (Gupta and Balakotaiah, 2001; Tronconi and Forzatti, 1992). It will be shown here that the presence of a washcoat around the circular flow areas does not alter the asymptotes but shifts the transition regime between them. It will also be shown that for channels with other flow geometries, where transverse diffusion is two-dimensional in nature, the asymptotic Sherwood number in the kinetic control regime depends on the relative washcoat diffusivity ( $\delta$ ), which reaches  $Sh_{H_1,\infty}$  of flow geometry for no washcoat diffusional limitations and  $Sh_{H_2,\infty}$  of the corresponding flow geometry in the limit of very strong washcoat diffusional limitations ( $\delta \rightarrow \infty$  with  $\phi_s^2 \delta \lambda > 1$ ). In the kinetic regime,  $Sh_\infty$  attains a new asymptote for  $\delta \gg 1$  with  $\phi_s^2 \delta \lambda \sim 1$ , which depends strongly on the washcoat geometry. This asymptote has not been reported in the literature. In the mass transfer controlled regime,  $Sh_\infty$  will be shown to be independent of the washcoat profile, which asymptotically approaches the  $Sh_{T,\infty}$  of flow geometry as  $\phi_s^2$  goes to  $\infty$ . In such geometries the variation of  $Sh_\infty$  from one asymptote to the other is nonmonotonic with respect to washcoat properties.

## Mathematical Model Formulation

We start with the assumption that all channels of the monolith are equivalent with uniform flow distribution and represent the whole matrix by a single straight channel. The active material is assumed to be dispersed uniformly within the porous washcoat deposited on the inner wall of the channel. In this analysis, we do not impose any restriction on the geometric shape of the channel, except that the cross section of the channel is invariant with the axial position, and allow the

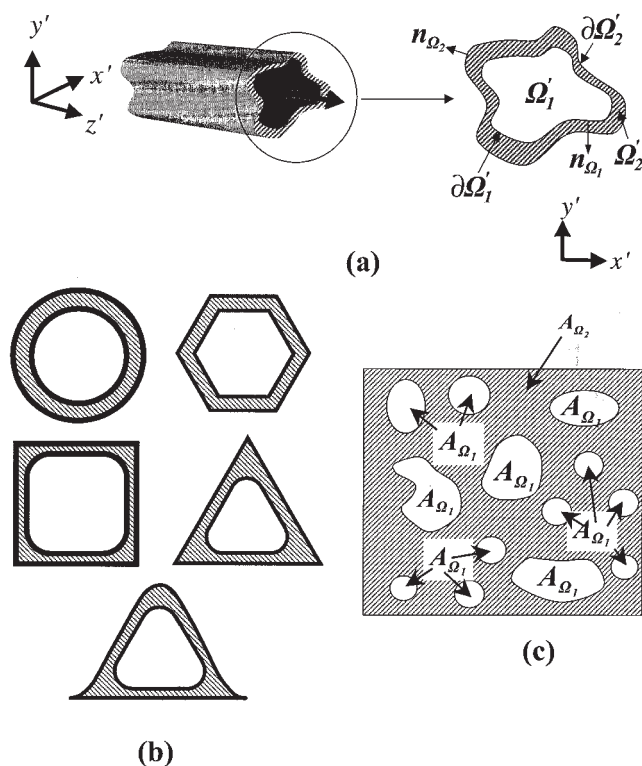


**Figure 1. (a) Diagram and notations used for a monolithic channel of arbitrary shape with nonuniform washcoat; (b) commonly used channel shapes and washcoat profiles; (c) nonuniform and irregular channels for which the theory described here can be extended.**

washcoat thickness to vary along the circumferential perimeter, as shown in the schematic diagram (Figure 1a). This represents more realistic monoliths with sharp corners used in the practical applications, where the washcoat tends to deposit more at the corners, such as square, triangular, hexagonal, or sinusoids (shown in Figure 1b), making the washcoat thickness nonuniform along the periphery. Other assumptions associated with the model equations are as follows:

- (1) The flow is laminar and fully developed.
- (2) The aspect ratio of the channel is assumed to be small; that is, the hydraulic diameter is much smaller than the length of the channel (which is true for most of the monoliths in practical applications). This assumption justifies the use of fully developed velocity profile within the channel and also leads to the simplification of negligible axial diffusion in both fluid phase and washcoat compared to the convective transport rate.
- (3) The inlet concentration of the reactant is assumed to be low enough to keep the temperature increase small, which in turn ensures the isothermality of the channel.
- (4) The variations of physical properties (such as density, viscosity, diffusivities, and so on) and velocity with temperature and compositions are neglected.

With the above assumptions, the steady-state variations of the reactant concentration within the fluid phase and washcoat can be described by the following coupled convection–diffusion–reaction equations

$$\langle u \rangle f(x', y') \frac{\partial C_1}{\partial z'} = D_m \nabla_*^2 C_1 \quad 0 < z' < L \quad (x', y') \in \Omega'_1 \quad (1a)$$

$$D_e \nabla_*^2 C_2 = k_r R(C_2) \quad 0 < z' < L \quad (x', y') \in \Omega'_2 \quad (1b)$$

where  $\Omega'_1$  and  $\Omega'_2$  denote the cross-sectional domains of the fluid phase and washcoat, respectively;  $L$  is the length of the channel; and  $\nabla_*^2$  is the transverse Laplacian operator in  $\Omega'_1$  and  $\Omega'_2$ . Here,  $C_1$  is the reactant concentration in the fluid phase,  $C_2$  is the reactant concentration within the washcoat,  $D_m$  is the molecular diffusivity of the reacting species in the fluid phase,  $D_e$  is the effective diffusivity of the reacting species within the washcoat,  $k_r$  is the intrinsic reaction rate constant based on unit washcoat volume,  $\langle u \rangle$  is the average velocity, and  $f(x', y')$  is the local velocity profile within the channel. The term  $R(C_2)$  in Eq. 1b represents the functional dependency of the reaction rate on reactant concentration and is equal to  $C_2$  for a first-order reaction. Note that the reaction rate becomes a function of both concentration and temperature for nonisothermal operation and the mass balance equations are coupled to the energy balance equations through this term. In this section, we retain the reaction rate in the form of  $R(C_2)$  to maintain the generality of the model. However, in the later sections we will consider a first-order reaction, given that the asymptotic mass transfer coefficients are insensitive to the functional form of  $R(C_2)$ . Equations 1a and 1b are subject to the no flux condition at the outer boundary of the channel ( $\partial\Omega'_2$ ) and the interfacial concentration and flux continuity conditions given by

$$\mathbf{n}_{\Omega_2} \cdot \nabla_* C_2 = 0 \quad \text{on } \partial\Omega'_2 \quad (1c)$$

$$C_1 = C_2 \quad \text{and} \quad \mathbf{n}_{\Omega_1} \cdot (D_m \nabla_* C_1 - D_e \nabla_* C_2) = 0 \quad \text{on } \partial\Omega'_1 \quad (1d)$$

and the inlet condition is given by

$$@ z' = 0 \quad C_1 = C^{in} \quad (x', y') \in \Omega'_1 \quad (1e)$$

where  $C^{in}$  is the inlet reactant concentration. Here,  $\partial\Omega'_1$  is the interfacial perimeter between the fluid phase and the washcoat,  $\partial\Omega'_2$  is the outer boundary of the channel,  $\mathbf{n}_{\Omega_1}$  is the unit outward normal to  $\partial\Omega'_1$ , and  $\mathbf{n}_{\Omega_2}$  is the unit outward normal to  $\partial\Omega'_2$ , as shown in Figure 1a. The first boundary condition, Eq. 1c, relies on the assumption that the outer wall of the channel is impermeable to the reacting species, whereas Eq. 1d ensures perfect contact between the two phases. Note that Eqs. 1a–1e are valid for channels with continuous as well as discontinuous washcoat and, thus, the following formulation is applicable to any general washcoated monolith.

The characteristic length scale for any arbitrary domain is defined as the ratio of the flow volume to the wetted surface. Similarly, for any straight washcoated channel with arbitrary cross-sectional geometry, we can define two characteristic length scales for the transverse directions associated with the

fluid phase ( $R_{\Omega_1}$ ) and washcoat ( $R_{\Omega_2}$ ), respectively. The effective transverse length scale for the fluid phase  $R_{\Omega_1}$  is defined as the ratio of the total flow area ( $A_{\Omega_1} = \int_{\Omega_1} d\Omega'$ ) to the wetted perimeter ( $P_{\Omega_1}$ ), whereas the effective diffusion length for the washcoat  $R_{\Omega_2}$  is defined as the ratio of the washcoat cross-sectional area ( $A_{\Omega_2} = \int_{\Omega_2} d\Omega'$ ) to the interfacial perimeter,  $P_{\Omega_w} = \int_{\partial\Omega_1} d\Gamma'$ , where  $d\Gamma'$  is the arc length along the perimeter. Note that the interfacial perimeter ( $P_{\Omega_w}$ ) is equal to the wetted perimeter ( $P_{\Omega}$ ) for the case of continuous washcoat and differs from  $P_{\Omega}$  for the discontinuous washcoat. In this analysis, we will illustrate the examples of continuous washcoat and thus will use  $P_{\Omega_w} = P_{\Omega}$  for the rest of the discussion. Nevertheless, the formulation remains the same, irrespective of the washcoat profile. [Remark: The transverse diffusion length for the fluid phase ( $R_{\Omega_1}$ ) is related to the hydraulic diameter of the channel by  $d_h = 4R_{\Omega_1}$ .]

Using  $R_{\Omega_1}$  and  $L$  as the length scales to normalize transverse and axial coordinates, respectively, and  $C_R$  as the reference concentration, we obtain four timescales in the system associated with convection ( $t_c$ ), transverse diffusion in the fluid phase ( $t_{\perp}^f$ ), transverse diffusion within washcoat ( $t_{\perp}^w$ ), and reaction ( $t_R$ )

$$t_c = \frac{L}{\langle u \rangle} \quad t_{\perp}^f = \frac{R_{\Omega_1}^2}{D_m} \quad t_{\perp}^w = \frac{R_{\Omega_2}^2}{D_e} \quad t_R = \frac{C_R}{k_v R(C_R)}$$

A combination of these time scales leads to four independent dimensionless parameters: transverse Peclet number (P), Damköhler number (Da), ratio of diffusivities ( $\delta$ ), and ratio of transverse diffusion lengths ( $\lambda$ ), given by

$$P = \frac{t_{\perp}^f}{t_c} = \frac{R_{\Omega_1}^2 \langle u \rangle}{D_m L} \quad Da = \frac{t_c}{t_R} = \frac{k_v R(C_R) L}{\langle u \rangle C_R} \quad \delta = \frac{D_m}{D_e} \quad \lambda = \frac{R_{\Omega_2}}{R_{\Omega_1}}$$

where the transverse Peclet number P is the ratio of transverse diffusion time in the fluid phase to the convection time, the Damköhler number Da is the ratio of the convection time to the reaction time,  $\delta$  is the ratio of the reactant diffusivity in the fluid phase to that in the washcoat, and  $\lambda$  is the ratio of the effective transverse diffusion length for the washcoat to that for the fluid phase. [Remark: In practice the diffusivity of the reactant within the washcoat is significantly lower than that in the fluid phase, making the parameter  $\delta$  much greater than 1 for all practical purposes, whereas the limit of  $\delta \ll 1$  is of interest for the case of heat transfer. We note that  $\delta$  depends strongly on various washcoat properties (such as pore dimensions, tortuosity, porosity, and so on) and is of order 10 when the washcoat diffusion is in the bulk regime. On the other hand, if diffusion within the washcoat is in the Knudsen regime,  $\delta$  can be in the range of 10 to 100.] Other dimensionless numbers that will appear in the following discussions are washcoat Thiele modulus,  $\phi^2 = R_{\Omega_2}^2 k_v R(C_R) / D_e C_R$ , defined as the ratio of the transverse diffusion time for the washcoat to the reaction time, and the local Damköhler number  $Da_{loc} = R_{\Omega_1} R_{\Omega_2} k_v R(C_R) / D_m C_R = t_{\perp}^f \lambda / t_R$ .  $Da_{loc}$  is also known as surface Thiele modulus ( $\phi_s^2$ ) in the chemical engineering literature and is related to the washcoat Thiele modulus as  $\phi^2 = \phi_s^2 \delta \lambda$ . Another relevant dimensionless parameter for describing the flow in a channel is the aspect ratio  $\alpha = 4R_{\Omega_1} / L$ , which also plays a significant role in determining the relative importance of various

terms in the balance equations. For example, the axial diffusion is negligible if  $\alpha \ll 1$ .

Using  $C^{in}$  as the reference concentration and defining the following dimensionless variables

$$c_1 = \frac{C_1}{C^{in}} \quad c_2 = \frac{C_2}{C^{in}} \quad x = \frac{x'}{R_{\Omega_1}} \quad y = \frac{y'}{R_{\Omega_1}} \quad z = \frac{z'}{L}$$

$$g(x, y) = f(R_{\Omega_1} x', R_{\Omega_1} y') \quad r(c_2) = \frac{R(C_2)}{R(C^{in})}$$

Equations 1a–e may be written in dimensionless form as

$$g(x, y) \frac{\partial c_1}{\partial z} = \frac{1}{P} \nabla^2 c_1 \quad 0 < z < 1 \quad (x, y) \in \Omega_1 \quad (2a)$$

$$Da \, r(c_2) = \frac{1}{\delta P} \nabla^2 c_2 \quad 0 < z < 1 \quad (x, y) \in \Omega_2 \quad (2b)$$

$$\mathbf{n}_{\Omega_2} \cdot \nabla c_2 = 0 \quad \text{on } \partial\Omega_2 \quad (2c)$$

$$\mathbf{n}_{\Omega_1} \cdot \left( \nabla c_1 - \frac{1}{\delta} \nabla c_2 \right) = 0 \quad \text{on } \partial\Omega_1 \quad \left. \begin{array}{l} c_1 = c_2 \quad \text{on } \partial\Omega_1 \end{array} \right\} \quad (2d)$$

$$@ \, z = 0 \quad c_1 = 1 \quad (2e)$$

where  $\Omega_1$ ,  $\Omega_2$ ,  $\partial\Omega_1$ , and  $\partial\Omega_2$  represent the dimensionless form of the respective quantities with superscript prime. Here,  $\nabla^2$  is the dimensionless transverse Laplacian operator and  $g(x, y)$  is the dimensionless fully developed velocity profile, normalized with respect to the average velocity, which can be obtained by solving the appropriate momentum balance equations within the flow area  $\{(x, y) \in \Omega_1\}$ . A more popular form of the washcoat equation, which has been used frequently in the engineering literature, is given by

$$\nabla^2 c_2 = \frac{\phi^2}{\lambda^2} r(c_2) \quad 0 < z < 1 \quad (x, y) \in \Omega_2$$

Equations 2a and 2e constitute the 2 or 3-D convection–diffusion model, which describes the variations of the reactant concentration in the flow area. Note that Eq. 2a is coupled with the washcoat equation by the interfacial continuity conditions, Eq. 2d. In the literature, this coupling has often been simplified by introducing an effectiveness factor  $\eta$ , which is defined as the ratio of the actual reaction rate averaged over the volume of the washcoat to the reaction rate evaluated at the fluid–washcoat interface and is given by

$$\eta = \frac{\int_{\Omega_2} R(C_2) d\Omega'}{A_{\Omega_2} R(C_2)|_{\partial\Omega_1}} \quad (3)$$

This approach inherits the assumption of constant concentration along the circumferential perimeter ( $\partial\Omega_1$ ) and solves the local washcoat equation (Eq. 2b) by imposing a Dirichlet



boundary condition on  $\partial\Omega_1$ . This solution is then related to the flux at the solid–fluid interface as

$$\mathbf{n}_{\Omega_1} \cdot \nabla c_1 = -\eta \phi_s^2 r(c_1) \equiv -\eta \phi_s^2 c_1 \quad (\text{for first-order reaction}) \quad \text{on } \partial\Omega_1 \quad (4)$$

This completes the description of the convection–diffusion model by providing the required boundary conditions in terms of only fluid-phase concentration. It is apparent that this approach significantly reduces the computational effort. However, there is no justification for the use of constant circumferential concentration while solving the washcoat equation, especially for monoliths with sharp corners or with nonuniform washcoat thickness.

## Two-Phase Model: Sherwood or Nusselt Number

The two-phase model describes the variations of the fluid-phase cup-mixing concentration along the length of the reactor, where the transverse gradients are expressed as an exchange of material between the cup-mixing and surface concentrations (lumping the transport resistances in a transfer coefficient). In this model, the steady-state averaged fluid-phase balance equation is written as

$$\langle u \rangle \frac{dC_m}{dz'} = -k_c a_v (C_m - C_s) \quad (5)$$

where  $k_c$  is the mass-transfer coefficient between the bulk fluid phase and substrate and  $a_v$  is the total interfacial area per unit flow volume,  $a_v = P_{\Omega}/A_{\Omega_1} = 1/R_{\Omega_1}$ . Here, the fluid phase cup-mixing concentration ( $C_m$ ) is defined as the transverse averaged concentration weighted with respect to the normalized longitudinal velocity [ $=f(x', y')$ ] and is given by

$$C_m = \frac{\int_{\Omega_1} f(x', y') C_1(x', y') d\Omega'}{\int_{\Omega_1} f(x', y') d\Omega'} \quad (6)$$

whereas the surface concentration  $C_s$  is the circumferentially averaged concentration at the fluid–solid interface

$$C_s = \frac{\int_{\partial\Omega_1} C_1(x', y') d\Gamma'}{\int_{\partial\Omega_1} d\Gamma'} \equiv \frac{\int_{\partial\Omega_1} C_2(x', y') d\Gamma'}{\int_{\partial\Omega_1} d\Gamma'} \quad (7)$$

Using the same dimensionless variables as in the full model, Eq. 5 can be rewritten in the following dimensionless form

$$\frac{dc_m}{dz} = -\frac{Lk_c}{\langle u \rangle R_{\Omega_1}} (c_m - c_s) \quad (8)$$

where the dimensionless cup-mixing and surface concentrations are given by

$$c_m = \frac{\int_{\Omega_1} g(x, y) c_1(x, y) d\Omega}{\int_{\Omega_1} g(x, y) d\Omega} \quad c_s = \frac{\int_{\partial\Omega_1} c_1(x, y) d\Gamma}{\int_{\partial\Omega_1} d\Gamma}$$

Note that, because of the scaling chosen here  $\int_{\Omega_1} g(x, y) d\Omega = \int_{\Omega_1} d\Omega$  and also  $\int_{\Omega_1} d\Omega = \int_{\partial\Omega_1} d\Gamma$ . To relate the mass transfer coefficient in the two-phase model to the derivable quantity associated with the full model (such as interfacial flux), Eq. 2a is integrated over the cross section  $\Omega_1$ , to obtain

$$\frac{dc_m}{dz} = \frac{1}{P \int_{\Omega_1} g(x, y) d\Omega} \int_{\partial\Omega_1} \mathbf{n}_{\Omega_1} \cdot \nabla c_1 d\Gamma \quad (9)$$

Comparing Eqs. 8 and 9, we can write

$$\frac{k_c R_{\Omega_1}}{D_m} = -\frac{\int_{\partial\Omega_1} \mathbf{n}_{\Omega_1} \cdot \nabla c_1 d\Gamma / \int_{\partial\Omega_1} d\Gamma}{(c_m - c_s)} \quad (10)$$

where  $k_c R_{\Omega_1}/D_m$  is the ratio of transverse diffusion time to mass transfer time from bulk to the fluid–solid interface and is related to the Sherwood number as  $Sh = k_c d_h/D_m$ , where  $d_h (=4R_{\Omega_1})$  is the hydraulic diameter of the channel. Hence, we obtain

$$Sh = \frac{4k_c R_{\Omega_1}}{D_m} = -\frac{4 \int_{\partial\Omega_1} \mathbf{n}_{\Omega_1} \cdot \nabla c_1 d\Gamma / \int_{\partial\Omega_1} d\Gamma}{(c_m - c_s)} \quad (11)$$

Using Eqs. 2b and 2d, the Sherwood number can be redefined as

$$Sh = \frac{4\phi_s^2 \int_{\Omega_2} r(c_2) d\Omega / \int_{\partial\Omega_1} d\Gamma}{\lambda(c_m - c_s)} \quad (12)$$

Equation 11 not only defines the Sherwood number but also, together with Eq. 8, completes the two-phase model by relating the surface and cup-mixing concentrations

$$Sh(c_m - c_s) = 4\phi_s^2 \eta r(c_s) \quad (13)$$

These two equations (Eqs. 8 and 13) have been used extensively in the prior literature to determine the  $Sh$  number experimentally. Note that Eq. 13 needs an appropriate value for the effectiveness factor  $\eta$ , which requires the solution of diffusion–reaction problem within the washcoat. However, because of the difficulty associated with the solutions of the two-dimensional diffusion–reaction equation in an arbitrary domain, the value of  $\eta$  has often been assumed to be unity, especially for a thin washcoat. This assumption may not be valid for monoliths with sharp corners, where catalysts tend to deposit more at the corners, increasing the diffusional limitations and thus decreasing the value of the overall effectiveness factor  $\eta$ . Thus, the use of this overpredicted effectiveness factor resulted in much lower values for the  $Sh$  (or  $Nu$ ) numbers (Bennett et al., 1991; Ullah et al., 1992; Votruba et al., 1975) than theoretically predicted values reported in the literature. This fact has been verified in previous work (Hayes and Kolaczowski, 1994), where it has been shown that the use of a proper value of  $\eta$  corresponding to the particular experimental conditions and washcoat geometry bounds the asymptotic Sherwood or Nusselt numbers within the limits of theoretical prediction.

## Analytical Solutions (for Linear Kinetics)

Let us consider the eigenvalue problem involving the Laplacian operator in domain  $\Omega = \Omega_1 \cup \Omega_2$  given by

$$\nabla^2 \Psi_{1,n} = -g(x, y) \mu_n \Psi_{1,n} \quad (x, y) \in \Omega_1 \quad (14a)$$

$$\frac{1}{\delta} \nabla^2 \Psi_{2,n} = P \text{ Da } \Psi_{2,n} \equiv \frac{\phi_s^2}{\lambda} \Psi_{2,n} \quad (x, y) \in \Omega_2 \quad (14b)$$

with the boundary conditions

$$\mathbf{n}_{\Omega_2} \cdot \nabla \Psi_{2,n} = 0 \quad \text{on } \partial\Omega_2 \quad (14c)$$

$$\mathbf{n}_{\Omega_1} \cdot \left( \nabla \Psi_{1,n} - \frac{1}{\delta} \nabla \Psi_{2,n} \right) = 0 \quad \text{on } \partial\Omega_1 \quad (14d)$$

where  $\mu_n$  is the  $n$ th eigenvalue and

$$\Psi_n = \begin{cases} \Psi_{1,n} & (x, y) \in \Omega_1 \\ \Psi_{2,n} & (x, y) \in \Omega_2 \end{cases}$$

is the corresponding  $n$ th eigenfunction in domain  $\Omega$ ,  $n = 1, 2, \dots, \infty$ . It can be easily shown that the above eigenvalue problem is self-adjoint with respect to the inner product

$$\langle \Psi_n, \Psi_m \rangle = \int_{\Omega_1} g(x, y) \Psi_{1,n} \Psi_{1,m} d\Omega + \int_{\Omega_2} g(x, y) d\Omega \quad (15)$$

and all eigenvalues are nonnegative ( $\mu_n \geq 0$ ,  $n = 1, 2, \dots$ ). Also, the eigenfunctions  $\Psi_n$ ,  $n = 1, 2, \dots, \infty$  satisfy the following orthogonality condition

$$\langle \Psi_m, \Psi_n \rangle = 0 \quad \text{if } m \neq n \quad \text{and} \quad \langle \Psi_m, \Psi_n \rangle \neq 0 \quad \text{if } m = n \quad (16)$$

Then, using the eigenfunction expansion, the solutions of Eqs. 2a–e, for any arbitrary cross-sectional channel with first-order catalytic reaction can be written as

$$c_1 = \sum_{n=1}^{\infty} \beta_n \exp\left(-\frac{\mu_n z}{P}\right) \Psi_{1,n} \quad \text{and} \quad c_2 = \sum_{n=1}^{\infty} \beta_n \exp\left(-\frac{\mu_n z}{P}\right) \Psi_{2,n} \quad (17)$$

where the  $n$ th Fourier constant  $\beta_n$  is given by

$$\beta_n = \frac{\langle 1, \Psi_n \rangle}{\langle 1, \Psi_n^2 \rangle} \quad (18)$$

Equation 17, after multiplying with the dimensionless velocity profile  $g(x, y)$  and integrating over cross-sectional domain  $\Omega_1$ ,

leads to the following expression for the cup-mixing concentration  $c_m$

$$c_m = \sum_{n=1}^{\infty} \beta_n \exp\left(-\frac{\mu_n z}{P}\right) \langle \Psi_{1,n}, 1 \rangle \equiv \sum_{n=1}^{\infty} \beta_n \exp\left(-\frac{\mu_n z}{P}\right) \langle \Psi_n, 1 \rangle \quad (19)$$

whereas integration of Eq. 17 over the circumferential perimeter gives the averaged surface concentration  $c_s$  as

$$c_s = \sum_{n=1}^{\infty} \frac{\beta_n}{\int_{\partial\Omega_1} d\Gamma} \exp\left(-\frac{\mu_n z}{P}\right) \int_{\partial\Omega_1} \Psi_{1,n} d\Gamma \quad (20)$$

These two expressions together with the definition of Sherwood number results in

$$\text{Sh} = \frac{4\phi_s^2 \sum_{n=1}^{\infty} \beta_n \exp\left(-\frac{\mu_n z}{P}\right) \int_{\Omega_2} \Psi_{2,n} d\Omega}{\omega \int_{\partial\Omega_1} d\Gamma \sum_{n=1}^{\infty} \beta_n \exp\left(-\frac{\mu_n z}{P}\right) \left( \langle \Psi_{1,n}, 1 \rangle - \frac{\int_{\partial\Omega_1} \Psi_{1,n} d\Gamma}{\int_{\partial\Omega_1} d\Gamma} \right)} \quad (21)$$

or equivalently

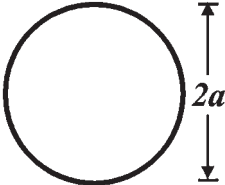
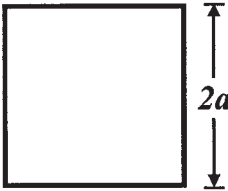
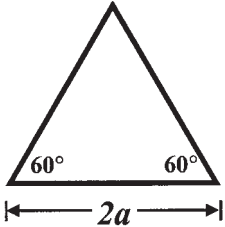
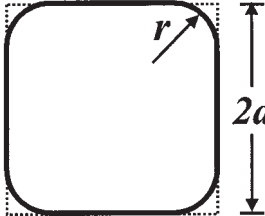
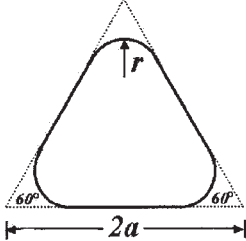
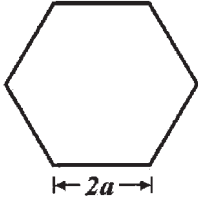
$$\text{Sh} = \frac{4 \sum_{n=1}^{\infty} \beta_n \exp\left(-\frac{\mu_n z}{P}\right) \int_{\partial\Omega_1} \mathbf{n}_{\Omega_1} \cdot \nabla \Psi_{1,n} d\Gamma}{\int_{\partial\Omega_1} d\Gamma \sum_{n=1}^{\infty} \beta_n \exp\left(-\frac{\mu_n z}{P}\right) \left( \langle \Psi_{1,n}, 1 \rangle - \int_{\partial\Omega_1} \Psi_{1,n} d\Gamma / \int_{\partial\Omega_1} d\Gamma \right)} \quad (22)$$

[Remark: The definition for the Sherwood number given by Eq. 21 is preferred over Eq. 22 in the numerical computations. The reason is that, for most cases, the concentration can be calculated more accurately than the flux at the solid–fluid interface. Computation of fluxes with the same order of accuracy as that of the concentration (such as using Hermite polynomial approximation) increases the numerical effort by an order of magnitude. Therefore, the definition given by Eq. 21 will be followed hereafter.] As can be observed from Eq. 21, the Sherwood number is a function of the axial position  $z$  and varies along the length of the channel as the concentration profile develops. That is, the mass transfer coefficient or  $\text{Sh}$ , which has a higher value in the entry region of the channel where the concentration boundary layer is developing, decreases along the length of the channel approaching an asymptotic value  $\text{Sh}_{\infty}$  as  $z$  approaches the concentration entry length ( $z/P \gg 1$ ). This asymptotic value corresponds to the fully developed concentration profile and is obtained by taking the limit  $z/P \gg 1$

$$\text{Sh}_{\infty} = \frac{4\phi_s^2 \int_{\Omega_2} \Psi_{2,1} d\Omega}{\lambda \left( \langle \Psi_{1,1}, 1 \rangle - \int_{\partial\Omega_1} \Psi_{1,1} d\Gamma / \int_{\partial\Omega_1} d\Gamma \right) \int_{\partial\Omega_1} d\Gamma} \quad (23)$$

Using the scaling factors used in this work, Eq. 23 can be manipulated and rewritten as

Table 1. Effective Diffusion Length and Asymptotic Sherwood Numbers for Some Common Channel Shapes

Channel Shape	$R_{\Omega_1}$	$(\text{Nu/Sh})_{H_2, \infty}$	$(\text{Nu/Sh})_{H_1, \infty}$	$(\text{Nu/Sh})_{T, \infty}$	$\alpha_{1, T}$
	$\frac{a}{2}$	4.364	4.364	3.656	0.81905
	$\frac{a}{2}$	3.089	3.608	2.977	0.80443
	$\frac{a}{2\sqrt{3}}$	1.893	3.111	2.497	0.77525
	$\frac{4(a^2 - r^2) + \pi r^2}{8(a - r) + 2\pi r}$	3.504 3.861 4.129 4.2998	3.896 4.114 4.252 4.332	3.219 3.412 3.545 3.625	0.80511 0.80861 0.81368 0.81770
	$\frac{\sqrt{3}r}{a}$ $\frac{\sqrt{3}a^2 - (3\sqrt{3} - \pi)r^2}{6a - 2(3\sqrt{3} - \pi)r}$	2.5799 3.276 3.836 4.207	3.598 3.998 4.224 4.319	2.891 3.243 3.479 3.603	0.77626 0.78471 0.80025 0.81383
	$\frac{\sqrt{3}}{2}a$	3.859	4.002	3.341	0.81557

$$\text{Sh}_{\infty} = \frac{4\phi_s^2 \int_{\Omega_2} \Psi_{2,1} d\Omega}{\lambda \left( \int_{\Omega_1} g(x, y) \Psi_{1,1} d\Omega - \int_{\partial\Omega_1} \Psi_{1,1} d\Gamma \right)} \quad (24)$$

It may be noted that, for monoliths with small aspect ratio ( $\alpha \ll 1$  or equivalently  $P \ll 1$ ), the entry length is much smaller than the channel length and we can use a constant Sherwood number ( $\text{Sh}_{\infty}$ ) for the entire channel.

It is a well-known fact that the asymptotic Sherwood number for circular or parallel-plate duct with wall reaction (that is, with negligible washcoat diffusional limitations), varies from

constant flux ( $\text{Sh}_{H, \infty}$ ) to constant concentration ( $\text{Sh}_{T, \infty}$ ) asymptote as  $\phi_s^2$  varies from 0 to  $\infty$  (Gupta and Balakotaiah, 2001; Tronconi and Forzatti, 1992). For these geometries, the constant flux asymptotes of first ( $\text{Sh}_{H, \infty}$ ) and second ( $\text{Sh}_{H_2, \infty}$ ) kind are the same because of the 1-D diffusion in the transverse direction, whereas they differ from each other for channels with other geometries, such as square, triangle, and so forth, where transverse diffusion is 2-D. Table 1 lists the values for the asymptotic Sherwood or Nusselt numbers for some commonly used channel geometries. The second column defines

the transverse diffusion length ( $R_{\Omega_1}$ ) for the channel; the third and fourth columns tabulate the asymptotic constant flux Sherwood numbers of second ( $Sh_{H_2,\infty}$ ) and first ( $Sh_{H_1,\infty}$ ) kind, respectively; and the fifth column lists the constant concentration or temperature ( $Sh_{T,\infty}$ ) asymptotes of the Sherwood or Nusselt number. [Remark: The relevance of various asymptotic Sherwood numbers to catalytic channels with wall reaction can easily be established by realizing the fact that the constant flux asymptotes are attained for channels with low catalyst loading ( $\phi_s^2 \ll 1$ ), whereas  $Sh_{T,\infty}$  is approached for channels with high catalyst loading ( $\phi_s^2 \gg 1$ ). For channels with low catalyst loading,  $Sh_\infty$  approaches  $Sh_{H_2,\infty}$  for uniform catalyst loading and  $Sh_{H_1,\infty}$  for nonuniform catalyst dispersion along the channel cross section (which is also true for channels with nonuniform washcoat thickness).] A systematic study on the influence of cross-sectional geometry on these asymptotic Sherwood (or Nusselt) numbers for straight channels with wall reaction is available in the heat-transfer literature (Shah and London, 1978), which, however, does not consider the presence of a washcoat.

In this work, we are interested in the effect of channel geometry on the asymptotic Sherwood numbers in presence of a washcoat and also on the effects of various washcoat parameters on these asymptotic values. We will present the results in the following order. First we will consider circular or parallel-plate channels with uniform washcoat thickness, where the bounds on the asymptotic Sherwood number will be shown analytically, and then we will consider the more realistic cases of monoliths with sharp corners and nonuniform washcoat thickness.

## Analytical and Numerical Results for $Sh_\infty$

### Uniform washcoat thickness: circular or parallel-plate geometries

In this section, we consider parallel-plate and circular channels with uniform washcoat thickness, as shown in Figures 2a and b,

respectively, where azimuthal symmetry is assumed to be preserved. In other words, the dispersion of the active metal within the washcoat is assumed to be uniform, resulting in unidirectional transverse diffusion within the channel. Consequently, defining the washcoat thickness to be  $a\varepsilon$ , where  $2a$  is either the diameter for a circular tube or the distance between the parallel plates, the associated eigenvalue problem can be simplified to

$$\frac{1}{\xi^i} \frac{d}{d\xi} \left( \xi^i \frac{d\psi_1}{d\xi} \right) = -\mu g(\xi) \psi_1 \quad 0 < \xi < 1 + i \quad (25)$$

$$\frac{d\psi_1}{d\xi} = 0 \quad @ \quad \xi = 0 \quad \text{and} \quad \frac{d\psi_1}{d\xi} = -\Phi_s^2 \psi_1 \quad @ \quad \xi = 1 + i \quad (26)$$

where  $i$  is 0 for parallel plate and is 1 for circular channel, and  $\xi$  is the dimensionless transverse coordinate, normalized with respect to the transverse diffusion length (which is  $a/2$  for circle and  $a$  for parallel plate), with origin at the center of the channel. The parameter  $\lambda$  can be expressed in terms of dimensionless washcoat thickness  $\varepsilon$  as

$$\lambda = \begin{cases} \varepsilon & \text{parallel plate} \\ 2\varepsilon + \varepsilon^2 & \text{circle} \end{cases}$$

Note that, Eqs. 25 and 26 are exactly the same as those for a channel with wall reaction, where the effect of washcoat diffusion is lumped in the parameter  $\Phi_s^2$ , which plays the same role as the surface Thiele modulus ( $\phi_s^2$ ) in the case of wall reaction. Thus, we call  $\Phi_s^2$  as the modified or effective Thiele modulus or local Damköhler number, which is given by

$$\Phi_s^2 = \begin{cases} \phi_s \tanh(\phi_s \sqrt{\delta\varepsilon}) / \sqrt{\delta\varepsilon} & \text{parallel plate} \\ \frac{\phi_s}{\sqrt{\delta(2\varepsilon + \varepsilon^2)}} \frac{K_1\left(\frac{2\phi_s}{\sqrt{(2\varepsilon + \varepsilon^2)/\delta}}\right) - \frac{K_1\left(\frac{2\phi_s(1+\varepsilon)}{\sqrt{(2\varepsilon + \varepsilon^2)/\delta}}\right)}{I_1\left(\frac{2\phi_s(1+\varepsilon)}{\sqrt{(2\varepsilon + \varepsilon^2)/\delta}}\right)} I_1\left(\frac{2\phi_s}{\sqrt{(2\varepsilon + \varepsilon^2)/\delta}}\right)}{K_0\left(\frac{2\phi_s}{\sqrt{(2\varepsilon + \varepsilon^2)/\delta}}\right) + \frac{K_1\left(\frac{2\phi_s(1+\varepsilon)}{\sqrt{(2\varepsilon + \varepsilon^2)/\delta}}\right)}{I_1\left(\frac{2\phi_s(1+\varepsilon)}{\sqrt{(2\varepsilon + \varepsilon^2)/\delta}}\right)} I_0\left(\frac{2\phi_s}{\sqrt{(2\varepsilon + \varepsilon^2)/\delta}}\right)} & \text{circular channel} \end{cases} \quad (27)$$

where  $I_j$  and  $K_j$  are the modified Bessel functions of order  $j$  ( $j = 0, 1$ ) with  $I$  and  $K$  representing the first and second kind, respectively. It may be noted that the effective surface Thiele modulus ( $\Phi_s^2$ ) becomes invariant of channel position for uniform catalyst dispersion within the washcoat. As mentioned earlier, the effective Thiele modulus accounts for the diffusion

within the washcoat, which can be explicitly shown by rewriting  $\Phi_s^2$  as

$$\Phi_s^2 = \phi_s^2 \eta \quad (28)$$

where  $\phi_s^2$  is the surface Thiele modulus without washcoat diffusional limitations and  $\eta$  is the effectiveness factor given by



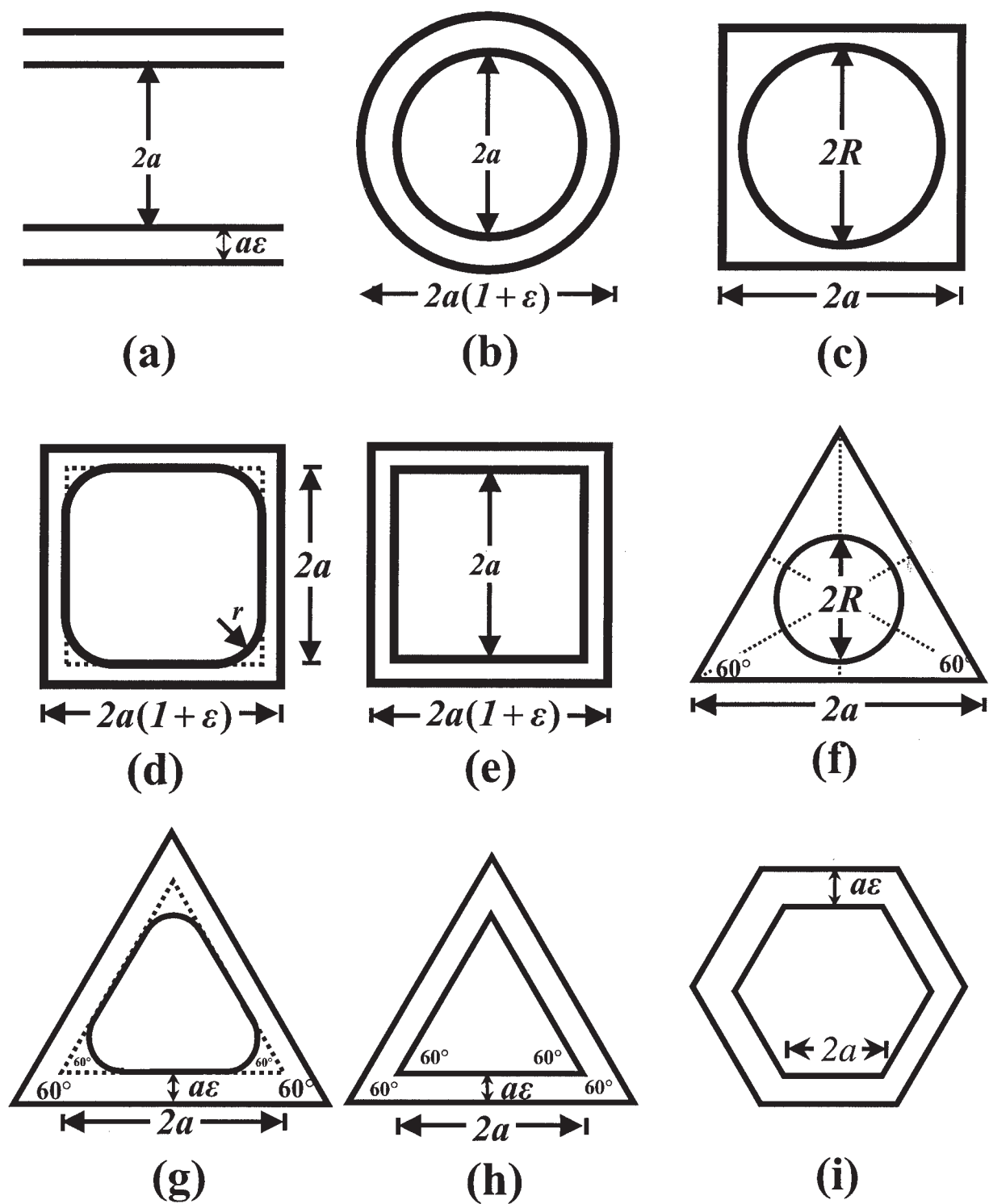


Figure 2. Diagram and dimensions of various channel and washcoat geometries considered in this work.

$$\eta = \begin{cases} \frac{\tanh(\phi)/\phi}{1 + \frac{K_1 \left( \frac{2\phi}{\varepsilon(2+\varepsilon)} \right) - \frac{K_1(2\phi(1+\varepsilon)/\varepsilon(2+\varepsilon))}{I_1(2\phi(1+\varepsilon)/\varepsilon(2+\varepsilon))} I_1 \left( \frac{2\phi}{\varepsilon(2+\varepsilon)} \right)} & \text{for parallel plate} \\ \frac{\phi}{\phi + \frac{K_0 \left( \frac{2\phi}{\varepsilon(2+\varepsilon)} \right) + \frac{K_1(2\phi(1+\varepsilon)/\varepsilon(2+\varepsilon))}{I_1(2\phi(1+\varepsilon)/\varepsilon(2+\varepsilon))} I_0 \left( \frac{2\phi}{\varepsilon(2+\varepsilon)} \right)} & \text{for circular channel} \end{cases} \quad (29)$$

Thus,  $\Phi_s^2$  captures the effect of washcoat diffusion through the effectiveness factor  $\eta$  as in the well-known effectiveness factor problem analyzed by Aris (1975). This also illustrates that for significant washcoat diffusion limitations ( $\eta \rightarrow 0$ ), the effective or apparent reaction rate is reduced and, as a result, the channel may be in a kinetically controlled regime despite the true reaction rate constant being high. Hence, the use of  $\eta = 1$  in such cases will underpredict the asymptotic Sherwood number by a factor of order  $\eta$ .

By solving Eqs. 25 and 26, the asymptotic Sherwood number for washcoated circular and parallel plate channels with unidirectional velocity field can be expressed as

$$\text{Sh}_\infty = \frac{4\Phi_s^2\mu_1}{\Phi_s^2 - \mu_1} \quad (30)$$

where  $\mu_1$  is the first eigenvalue associated with Eq. 25. For special case of flat velocity profile [ $g(\xi) = 1$ ], Eq. 25 can be solved analytically and  $\mu_1$  can be obtained as the first root of the characteristic equations given by

$$\sqrt{\mu} \tan(\sqrt{\mu}) = \Phi_s^2 \quad \text{for parallel plate} \quad (31a)$$

$$\sqrt{\mu} J_1(2\sqrt{\mu}) = \Phi_s^2 J_0(2\sqrt{\mu}) \quad \text{for circular channel} \quad (31b)$$

where  $J_0$  and  $J_1$  are the Bessel functions of order 0 and 1, respectively. [Remark: Although the local flow field of  $g(\xi) = 1$  is an idealized velocity profile that is approached in the limit of  $\text{Sc} \rightarrow 0$ , where  $\text{Sc}$  is the Schmidt number, it provides useful insight on the bounds of the asymptotic Sherwood number and its dependency on various system parameters.] For a flat velocity profile, it can be shown that in the limit of  $\Phi_s^2 \rightarrow 0$  (that is, in the kinetic regime), the first eigenvalue can be expressed as

$$\begin{aligned} \mu_1 &= \Phi_s^2 - \frac{1}{3} \Phi_s^4 + h.o.t. & (\text{parallel plate}) & \quad \text{and} \\ \mu_1 &= \Phi_s^2 - \frac{1}{2} \Phi_s^4 + h.o.t. & (\text{circular channel}) & \end{aligned} \quad (32)$$

whereas  $\mu_1$  in the mass-transfer controlled regime ( $\Phi_s^2 \gg 1$ ) is given by

$$\begin{aligned} \mu_1 &= \pi^2/4 & (\text{for parallel plate}) & \quad \text{and} \\ \mu_1 &= 5.7832/4 & (\text{for circular channel}) & \end{aligned} \quad (33)$$

Therefore, the constant flux and constant concentration (or temperature) asymptotes of the Sherwood number for washcoated circular and parallel plate channels with a flat velocity profile are obtained as

$$\begin{aligned} \text{Sh}_{H,\infty} &= \begin{cases} 12 \\ 8 \end{cases} \quad \text{and} \\ \text{Sh}_{T,\infty} &= 4\mu_1 = \begin{cases} \pi^2 & \text{for parallel plate} \\ 5.7832 & \text{for circular channel} \end{cases} \end{aligned} \quad (34)$$

Similarly, for a fully developed velocity profile, with  $g(\xi) = 2(1 - \xi^2)$  for circular channel and  $3(1 - \xi^2)/2$  for parallel plate, the first eigenvalue  $\mu_1$  can be determined in the limit of kinetic ( $\Phi_s^2 \rightarrow 0$ ) and mass transfer ( $\Phi_s^2 \rightarrow \infty$ ) controlled regime by asymptotic expansion and is given by

$$\begin{aligned} \mu_1 &= \begin{cases} \Phi_s^2 - \frac{17}{35} \Phi_s^4 + h.o.t. & \Phi_s^2 \ll 1 \\ \Phi_s^2 - \frac{11}{12} \Phi_s^4 + h.o.t. & \Phi_s^2 \ll 1 \end{cases} \quad \text{and} \\ & \begin{aligned} 1.8852 \quad \Phi_s^2 \gg 1 & \quad \text{for parallel plate} \\ 0.9142 \quad \Phi_s^2 \gg 1 & \quad \text{for circular channel} \end{aligned} \end{aligned} \quad (35)$$

This results in the following asymptotes of the Sherwood number in washcoated circular and parallel plate channels with a fully developed velocity profile

$$\begin{aligned} \text{Sh}_{H,\infty} &= \begin{cases} 8.235 \\ 4.3636 \end{cases} \quad \text{and} \\ \text{Sh}_{T,\infty} &= 4\mu_1 = \begin{cases} 7.54072 & \text{parallel plate} \\ 3.6568 & \text{circular channel} \end{cases} \end{aligned} \quad (36)$$

It can be observed from the above analysis that the asymptotic Sherwood number is independent of the washcoat properties and attains the corresponding wall reaction asymptotes (of the flow geometry), as expected from Eqs. 25 and 26, which clearly illustrate the equivalence between the two cases. In other words, the asymptotic Sherwood number for circular and parallel-plate channels with uniform washcoat distribution is bounded by the constant flux and constant temperature asymptotes of corresponding geometry and varies smoothly from one to the other as  $\Phi_s^2$  varies from 0 to  $\infty$ . The dependency of  $\text{Sh}_\infty$  on the washcoat profile comes only through the effective surface Thiele modulus, which determines the transition between the asymptotes, which occurs at  $\Phi_s^2 \sim 1$ . Therefore, the transition region between  $\text{Sh}_{H,\infty}$  and  $\text{Sh}_{T,\infty}$  asymptotes is a function of washcoat parameters  $\delta$  and  $\lambda$  and shifts to a higher  $\Phi_s^2$  for larger  $\delta$  and/or  $\lambda$ . This is attributed to an increase in the

**Table 2. Effective Diffusion Lengths for Some Washcoated Channel Geometries**

Channel Shape	$R_{\Omega_1}$	$R_{\Omega_2}$
Figure 2a	$a$	$a\varepsilon$
Figure 2b	$\frac{a}{2}$	$\frac{a\varepsilon(\varepsilon + 2)}{2}$
Figure 2c	$\frac{R}{2}$	$\frac{2a^2}{\pi R} - \frac{R}{2}$
Figure 2d	$\frac{4(a^2 - r^2) + \pi r^2}{8(a - r) + 2\pi r}$	$\frac{4a^2(2\varepsilon + \varepsilon^2) + (4 - \pi)r^2}{8(a - r) + 2\pi r}$
Figure 2e	$\frac{a}{2}$	$\frac{a\varepsilon(\varepsilon + 2)}{2}$
Figure 2f	$\frac{R}{2}$	$\frac{\sqrt{3} a^2 - \pi R^2}{2\pi R}$
Figure 2g	$\frac{a - (3 - \pi/\sqrt{3})r^2/a}{2\sqrt{3} - 2(3 - \pi/\sqrt{3})r/a}$	$\frac{\sqrt{3}a\varepsilon(\sqrt{3}\varepsilon + 2) + (3 - \pi/\sqrt{3})r^2/a}{2\sqrt{3} - 2(3 - \pi/\sqrt{3})r/a}$
Figure 2h	$\frac{a}{2\sqrt{3}}$	$\frac{a(3\varepsilon^2 + 2\sqrt{3}\varepsilon)}{2\sqrt{3}}$
Figure 2i	$\frac{\sqrt{3} a}{2}$	$\frac{(\varepsilon^2 + 2\sqrt{3}\varepsilon)a}{2\sqrt{3}}$

diffusional limitations within the washcoat or an equivalent reduction in the apparent reaction rate for the corresponding increases in  $\delta$  and  $\lambda$ . Therefore, for channels with either thicker or denser (low porosity) washcoat, the transition from constant flux to a constant temperature asymptote is delayed to a higher  $\phi_s^2$ , which also broadens the transition region in  $Sh_\infty$  vs.  $\phi_s^2$  plots.

### Nonuniform washcoat thickness

In this section, we consider the most commonly used channel shapes of squares, triangles, and hexagons, as shown in the schematic diagram (Figure 1b). In practice, during the coating of the channels, the washcoat tends to deposit more at the corners, leading to nonuniform washcoat thickness around the periphery of the channel. For example, in a square monolith, the thickness of the washcoat may be only 10  $\mu\text{m}$  at the side, but may be up to 150  $\mu\text{m}$  thick at the corner (Hayes and Kolaczowski, 1994). Accumulation of the coating material at the corner also smooths out the available flow area, resulting in a different cross-sectional geometry for the flow area than that of the channel. The expressions for the effective transverse diffusion lengths, associated with various flow area and washcoat geometries considered here, are given in Table 2, where the second column lists the effective transverse diffusion length for the flow area ( $R_{\Omega_1}$ ) and the third column tabulates the effective transverse diffusion length for the corresponding washcoat geometry ( $R_{\Omega_2}$ ). The asymptotic Sherwood numbers for various flow geometries are listed in Table 1 (as discussed earlier). The first approximation of any washcoated channel with corners is to consider the flow area to be circular.

Thus, first we consider a square channel with circular flow area and assume the flow within the channel to be fully developed. We use the finite-element package FEMLAB [version 2.3.0.145, Copyright 1994–2002 by COMSOL, Burlington, MA] to calculate the first eigenvalue and eigenfunctions of the associated eigenvalue problem (Eqs. 14a–14d). Then, the asymptotic Sherwood number for different  $\delta$ ,  $\lambda$ , and  $\phi_s^2$  values is

calculated using the definition (Eq. 23 or 24). This procedure has been adapted in all the following calculations. Asymptotic Sherwood numbers, as a function of local Damköhler number ( $\phi_s^2$ ) for a square channel of dimension  $2a$  with circular flow area of radius  $R$  (Figure 2c), are shown in Figure 3 for various  $\delta$  and  $\lambda$  values.

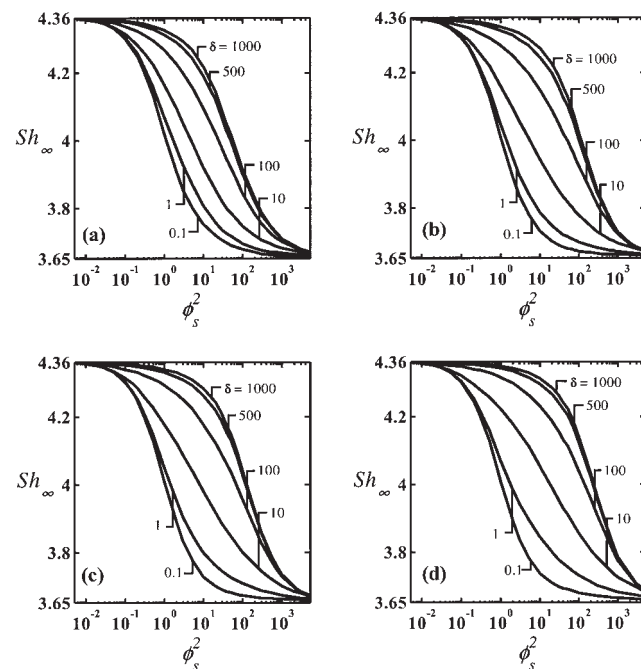


**Figure 3. Plot of asymptotic Sherwood number ( $Sh_\infty$ ) vs. surface Thiele modulus ( $\phi_s^2$ ) for a square channel with circular flow area and with fully developed velocity profile.**

Results are shown for  $\delta$  values in the range of 0.1 to 1000 for four different channel dimensions of  $a/R = 1.01$  in (a), 1.1 in (b), 1.2 in (c), and 1.5 in (d).

The results are plotted for four different channel dimensions of  $a/R = 1.01, 1.1, 1.2$ , and  $1.5$  corresponding to Figures 2a, b, c, and d, respectively. In each case, the results are shown for  $\delta$  within the range of 0.1 to 1000. As given in Table 2, the associated transverse diffusion lengths for a square monolith with circular flow area are given by

$$R_{\Omega_1} = \frac{R}{2} \quad \text{and} \quad R_{\Omega_2} = 2 \frac{a^2}{\pi R} - \frac{R}{2}$$

which can be used to calculate  $\lambda = (4/\pi)(a/R)^2 - 1$  for different channel dimensions used as  $\lambda = 0.3, 0.54, 0.83$ , and  $1.86$ , respectively. It may be noticed from the figure that the asymptotic Sherwood number is bounded by the same constant flux ( $Sh_{H,\infty} = 4.363$ ) and constant concentration ( $Sh_{T,\infty} = 3.6568$ ) asymptotes (of the flow geometry) as in the case of the wall reaction or uniform washcoat thickness. (As mentioned before  $Sh_{H,\infty} = Sh_{H,\infty}$  for circular geometry.) The presence of square or nonuniform washcoat does not influence these asymptotes, which was also observed in the previous example of uniform washcoat thickness.

In the kinetic regime ( $\phi_s^2 \ll 1$ ), where the characteristic reaction time is much higher than the transverse diffusion time, a nearly uniform concentration distribution is reached within the channel, resulting in constant flux around the fluid–solid interface. Similarly, at the other extreme of high catalyst loading ( $\phi_s^2 \gg 1$ ), where the reaction rate is instantaneous compared to molecular diffusion, the concentration at the solid–fluid interface goes to zero. Also, it is self-explanatory that in both the limits of large and small surface Thiele modulus, the presence of square or nonuniform washcoat influences neither the interfacial conditions discussed above nor the azimuthal symmetry present in the flow area. Therefore, the asymptotic Sherwood number for circular flow areas with nonuniform washcoat of various geometries (such as square, triangular, or hexagonal) is independent of the washcoat profiles and corresponds to the circular flow geometry, attaining  $Sh_{H,\infty}$  in the limit of  $\phi_s^2 \rightarrow 0$  and  $Sh_{T,\infty}$  for large  $\phi_s^2$ . However, as discussed in the previous example, the transition between the asymptotes depends on various washcoat parameters (such as  $\delta$ ,  $\lambda$ , and washcoat geometry) through the effective surface Thiele modulus. An increase in  $\delta$  or  $\lambda$  decreases the effective surface Thiele modulus by increasing the diffusional limitations within the washcoat and, thus, shifts the transition between the constant flux and concentration asymptotes to a higher  $\phi_s^2$ , which is observed in Figures 3a–3d. Also note that the transition region broadens as the thickness of the washcoat increases, which is self-explanatory from the above discussion.

It is now clear that for circular flow area, the asymptotic Sherwood number is independent of the washcoat shape and attains  $Sh_{H,\infty}$  and  $Sh_{T,\infty}$  (of circular geometry) as  $\phi_s^2$  varies from 0 to  $\infty$ . Therefore, the  $Sh_\infty$  vs.  $\phi_s^2$  plots for other channel geometries with circular flow area follow the same trends as observed in Figure 3 (the results are not shown here), except the fact that the transition from one asymptote to the other depends on the details of the washcoat profiles. [Remark: For most of the applications the asymptotic limits of  $Sh_\infty$  for  $\phi_s^2 \rightarrow 0$  and  $\phi_s^2 \rightarrow \infty$  are of practical interest, which are independent of the washcoat profiles.]

In the above examples, we have approximated the flow area

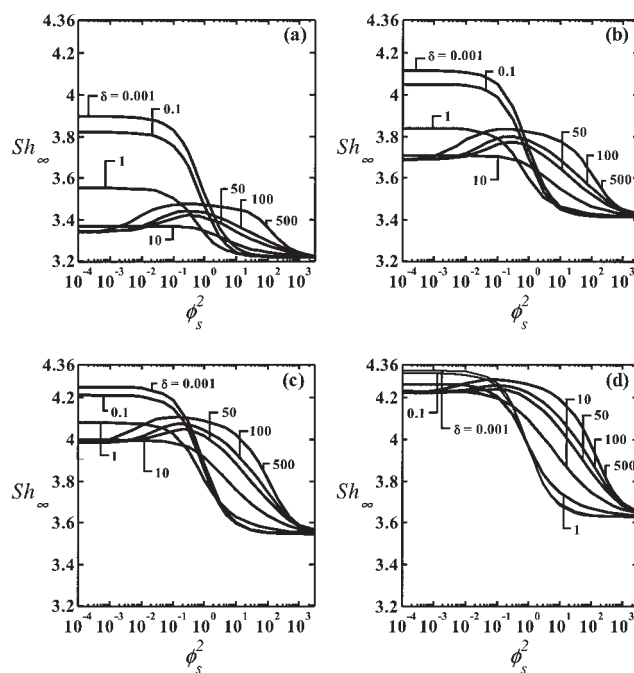


**Figure 4. Asymptotic Sherwood number ( $Sh_\infty$ ) vs. surface Thiele modulus ( $\phi_s^2$ ) for a square channel with rounded square flow area and with fully developed velocity profile.**

Results are shown for dimensionless washcoat thickness  $\varepsilon = 0.2$  and  $\delta$  values spanning the range of 0.001 to 500 for four different degrees of roundness of  $r/a = 0.2$  in (a), 0.4 in (b), 0.6 in (c), and 0.8 in (d).

to be circular. However, in practice nonuniform deposition of washcoat rounds the flow area only near the corner. Thus, the same geometric shape as the channel with rounded corners would be a better approximation for the flow area. For example, rounded square or triangle would be a closer approximation of the flow areas in a real washcoated monolith with square and triangular cross sections, respectively. First, we consider the case of a square monolith.

Figure 4 plots the  $Sh_\infty$  vs.  $\phi_s^2$  for a square monolith with rounded square flow area. The washcoated square monolith of dimension  $2a(1 + \varepsilon)$  is shown in Figure 2d, where  $2a$  is the dimension of the inside square with rounded corner of radius  $R$  and  $a\varepsilon$  is the thickness of the washcoat at the center of the channel. Here we have considered four different degrees of roundness, spanning the range of  $r/a = 0.2$  to 0.8. Figure 4a presents the results for  $r/a = 0.2$ , whereas (b), (c), and (d) present those for  $r/a$  values of 0.4, 0.6, and 0.8, respectively. In all cases, the dimensionless center washcoat thickness  $\varepsilon$  has been fixed to 0.2, whereas  $\delta$  has been varied from 0.001 to 500. Note that the geometry of the flow area for the case of  $r/a = 0.2$  is closer to a square, whereas it is more like a circle for  $r/a = 0.8$ , limiting to a perfect square at  $r/a = 0$  (which will be considered in the following example) and to a perfect circle at  $r/a = 1$  (which has already been considered). Using the expressions for the effective transverse diffusion lengths for the above geometry as given in Table 2, the parameter  $\lambda$  for various  $r/a$  values can be calculated from the following relation

$$\lambda = \frac{\left(\frac{a}{r}\right)^2 (2\varepsilon + \varepsilon^2) + 1 - \pi/4}{\left(\frac{a}{r}\right)^2 + \pi/4 - 1}$$

The difference between  $Sh_{H1,\infty}$  and  $Sh_{H2,\infty}$  for a rounded square (which reaches maximum in a perfect square,  $r/a = 0$ ) decreases with increasing degree of roundness (that is, increasing  $r/a$ ), and vanishes in the limit of  $r/a = 1$ , which corresponds to a circle. Various asymptotic Sherwood numbers for a rounded square are listed in Table 1, which along with Figure 4 illustrates the fact that both constant flux and concentration asymptotes increase with increasing  $r/a$ , approaching the corresponding circular geometry asymptotes for  $r/a = 1$ . Also note that for square geometry, constant flux asymptotes are always greater than the constant concentration asymptote as in the case of circular geometry.

It may be noticed from Figure 4 that  $Sh_\infty$  is independent of the washcoat profiles in the mass-transfer controlled regime and attains the corresponding constant concentration asymptote of the flow geometry at large  $\phi_s^2$ . For example,  $Sh_\infty$  for  $\phi_s^2 \rightarrow \infty$  reaches the value of 3.219 in Figure 4a (corresponding to a rounded square with  $r/a = 0.2$ ), whereas it approaches 3.625 in a square channel with  $r/a = 0.8$ , which are independent of the parameters  $\delta$  or  $\lambda$ . This is attributed to the fact that because the catalytic reaction rate is instantaneous, compared to the transverse diffusion, the reactant concentration goes to zero at the fluid–solid interface in the limit of  $\phi_s^2 \rightarrow \infty$ , which leads to a constant concentration distribution around the periphery of the channel. This remains unchanged along the length of the channel and is also uninfluenced by the presence of nonuniform washcoat, resulting in the insensitivity of the asymptotic Sherwood number on washcoat properties in the mass-transfer controlled regime, which approaches the constant concentration asymptote of the flow geometry.

In the kinetic regime ( $\phi_s^2 \rightarrow 0$ ), where the transverse diffusion in the fluid phase is much faster than the catalytic reaction occurring within the washcoat, the distribution of concentration around the periphery of the channel depends mainly on the parameter  $\delta$ , which determines the relative magnitude of diffusional limitations within the washcoat compared to the fluid phase. For no diffusional limitations within the washcoat ( $\delta \rightarrow 0$ ), concentration gradients within the washcoat become negligible and the fluid–solid interface remains at constant concentration or temperature. However, the 2-D diffusion within the washcoat results in a circumferentially nonuniform flux at the solid–fluid interface. Nevertheless, the total flux around the channel cross section remains constant along the length of the channel. It is obvious that in this limit concentration and the associated interfacial flux distributions are independent of the washcoat profile. Therefore, the asymptotic Sherwood number for low catalyst loading ( $\phi_s^2 \ll 1$ ) and no washcoat diffusional limitations ( $\delta \rightarrow 0$ ) becomes independent of the washcoat properties and reaches  $Sh_{H1,\infty}$  of corresponding flow area geometry.

On the other hand, for strong washcoat diffusional limitations, concentration gradients in the kinetic control regime are confined within the washcoat, whereas the extent of variations depends on the absolute magnitude of  $\phi_s^2 \delta \lambda$ , where finite gradients might be present within the washcoat for  $\phi_s^2 \delta \lambda \sim 1$ .

This results in a third asymptote for the Sherwood number in the limit of  $\phi_s^2 \ll 1$  but  $\phi_s^2 \delta \lambda \sim 1$  with  $\delta \gg 1$ , which depends strongly on the annular washcoat geometry (that is, both channel and flow area geometry). We denote this asymptote as  $Sh_{w,\infty}$ , which is always lower than the constant flux asymptotes and increases with increasing  $r/a$  (as other asymptotes, that is, constant flux and constant temperature), finally reaching the  $Sh_{H,\infty}$  of a circle for  $r/a = 1$ . However, the strong diffusion barriers within the washcoat in the limit of  $\delta \rightarrow \infty$  ( $\phi_s^2 \delta \lambda \gg 1$ ) result in zero flux around the channel and consequently  $Sh_\infty$  reaches  $Sh_{H2,\infty}$  (of flow geometry), which is independent of the washcoat properties for obvious reasons.

Therefore, for any washcoated channel other than circular geometry, if the washcoat pore structure is varied from a low ( $\phi \rightarrow 0$ ) to high packing ( $\delta \rightarrow \infty$ ), keeping the total catalyst loading fixed,  $Sh_\infty$  approaches  $Sh_{w,\infty}$  for  $\phi_s^2 \delta \lambda \lesssim 1$  with  $\delta \gg 1$  in the kinetic regime ( $\phi_s^2 \ll 1$ ), which moves to  $Sh_{H1,\infty}$  for  $\delta \rightarrow 0$  and to  $Sh_{H2,\infty}$  for  $\delta \rightarrow \infty$  with  $\phi_s^2 \delta \lambda \gg 1$ , whereas for high catalyst loading ( $\phi_s^2 \gg 1$ ),  $Sh_\infty$  is independent of  $\delta$  and reaches  $Sh_{T,\infty}$  (as can be observed from the figures).

Similarly, for a fixed washcoat structure (that is, fixed  $\delta$ ), if catalyst loading is varied from low ( $\phi_s^2 \ll 1$ ) to high ( $\phi_s^2 \gg 1$ ) density,  $Sh_\infty$  starts with  $Sh_{H1,\infty}$  at low catalyst loading ( $\phi_s^2 \ll 1$ ) in channels with no washcoat diffusion limitations ( $\delta \rightarrow 0$ ), which then decreases smoothly to  $Sh_T$  as catalyst loading is increased to  $\phi_s^2 \rightarrow \infty$ . On the other hand, for dense washcoat ( $\delta \gg 1$ ),  $Sh_\infty$  approaches  $Sh_{w,\infty}$  for  $\phi_s^2 \ll 1$  ( $\phi_s^2 \delta \lambda < 1$ ) and increases with  $\phi_s^2$  reaching  $Sh_{H2,\infty}$  for  $\phi_s^2 \sim 1$ , where  $\phi_s^2 \delta \lambda \gg 1$ . Then  $Sh_\infty$  decreases for any further increase in  $\phi_s^2$  and attains  $Sh_{T,\infty}$  for  $\phi_s^2 \rightarrow \infty$ . This results in nonmonotonic variations in the  $Sh_\infty$  vs.  $\phi_s^2$  plots for washcoat with strong washcoat diffusion limitations. For intermediate  $\delta$ ,  $Sh_\infty$  is bounded by the above asymptotes, but its variation with  $\phi_s^2$  depends on the details of washcoat properties, and so is the transition between the asymptotes for all cases.

As mentioned above, a similar kind of behavior is observed for triangular channel with rounded triangular flow area, as shown in Figure 5, which plots the asymptotic Sherwood number vs.  $\phi_s^2$  for triangular geometry. Assuming the dimension of the equilateral triangular channel to be  $2a(1 + \sqrt{3}\varepsilon)$ , where  $2a$  is the dimension of the inside triangle with the rounded corner of radius  $r$  and  $\varepsilon$  is the washcoat thickness at the center of the channel (Figure 2g), the dimensionless parameter  $\lambda$  can be expressed as

$$\lambda = \frac{3a^2(2\varepsilon + \sqrt{3}\varepsilon^2) + (3\sqrt{3} - \pi)r^2}{\sqrt{3}a^2 - (3\sqrt{3} - \pi)r^2}$$

In Figure 5, dimensionless washcoat thickness has been kept fixed at  $\varepsilon = 0.2$ , whereas  $r$  has been varied from  $\sqrt{3}r/a = 0.2$  to 0.8 with an increment of 0.2 from Figures 5a–d, respectively. In each case,  $Sh_\infty$  is plotted for various  $\delta$  values spanning the range of 0.001 to 500. From Table 1 and also from the figures, it is clear that the constant flux and concentration Sherwood numbers follow the same trend as that in the square geometry; that is,  $Sh_{H1,\infty}$ ,  $Sh_{H2,\infty}$ , and  $Sh_{T,\infty}$  increase with increasing  $r/a$  and reach the corresponding circular geometry asymptotes at  $\sqrt{3}r/a = 1$ . Also, the difference between  $Sh_{H1,\infty}$  and  $Sh_{H2,\infty}$  decreases with increasing degree of roundness, which finally vanishes in the limit of  $\sqrt{3}r/a \rightarrow 1$ .



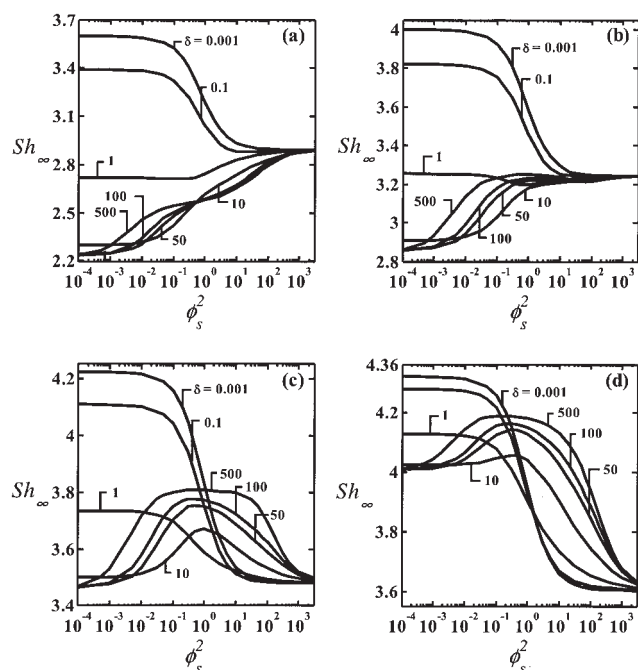


**Figure 5. Asymptotic Sherwood number ( $Sh_\infty$ ) vs. surface Thiele modulus ( $\phi_s^2$ ) for a triangular channel with rounded triangular flow area and with fully developed velocity profile.**

Results are shown for dimensionless washcoat thickness  $\varepsilon = 0.2$  and  $\delta$  values spanning the range of 0.001 to 500 for four different degrees of roundness of  $\sqrt{3} r/a = 0.2$  in (a), 0.4 in (b), 0.6 in (c), and 0.8 in (d).

However, unlike square geometry,  $Sh_{H_2,\infty}$  is lower than  $Sh_{T,\infty}$  for triangles with  $\sqrt{3} r/a < 0.4$ , whereas  $Sh_{H_1,\infty} > Sh_{T,\infty}$  for all  $r/a$  values.

Similar to the square geometry, in the kinetic regime  $Sh_\infty$  reaches  $Sh_{w,\infty}$  for  $\phi_s^2 \delta \lambda \sim 1$  and  $\delta \gg 1$ , which approaches  $Sh_{H_1,\infty}$  (of the particular flow geometry) for channels with no washcoat diffusion ( $\phi_s^2 \delta \lambda \ll 1$ ,  $\delta \ll 1$ ) and moves to  $Sh_{H_2,\infty}$  of the corresponding flow geometry in the limit of  $\delta \rightarrow \infty$  ( $\phi_s^2 \delta \lambda \gg 1$ ,  $\phi_s^2 \ll 1$ ). Thus, in the limit of  $\delta \rightarrow 0$ ,  $Sh_\infty$  decreases monotonically from  $Sh_{H_1,\infty}$  to  $Sh_{T,\infty}$  as the catalyst loading ( $\phi_s^2$ ) is changed from 0 to  $\infty$ , as observed in Figure 5. However, for large  $\delta$ ,  $Sh_\infty$  starts at  $Sh_{w,\infty}$  of the corresponding annular washcoat geometry in the limit of  $\phi_s^2 \rightarrow 0$  with  $\phi_s \delta \lambda < 1$  and approaches  $Sh_{H_2,\infty}$  of the flow geometry at around  $\phi_s^2 \sim 1$ , which then reaches  $Sh_{T,\infty}$  for high catalyst loading ( $\phi_s^2 \gg 1$ ). It may be noted that for  $\delta > 1$ , lower  $Sh_{H_2,\infty}$  than  $Sh_{T,\infty}$  for channels with  $\sqrt{3} r/a < 0.4$  results in a monotonic increase (with an inflection point) in the  $Sh_\infty$  with  $\phi_s^2$  (Figure 5a), whereas higher  $Sh_{H_2,\infty}$  creates a plateau around  $\phi_s^2 \sim 1$  in the  $Sh_\infty$  vs.  $\phi_s^2$  plots for  $\sqrt{3} r/a \geq 0.4$  (Figure 5b–d). For intermediate  $\delta$  values, the  $Sh_\infty$  lies between the asymptotes mentioned above, whereas their variations with  $\phi_s^2$  are functions of washcoat profile (such as  $\delta$ ,  $\lambda$ , and geometry) as well as the transition between the asymptotes, as illustrated in the earlier examples.

In the next examples we consider channels with corners where the flow area has the same geometric shape as that of the channel, which is the other extreme of approximation for

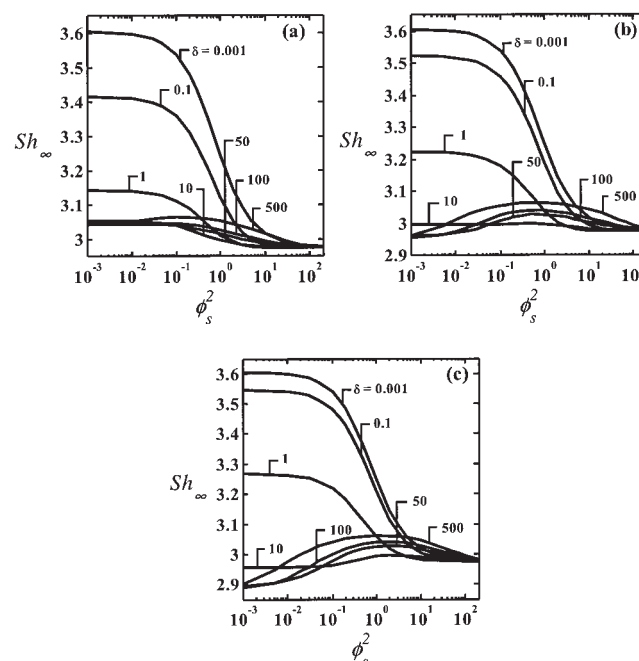
washcoated monoliths. Specifically we consider the cases of square and triangular channels with square and triangular flow areas, respectively. The results are shown in Figures 6 and 7.

Figure 6 plots the asymptotic Sherwood number for a square channel of dimension  $2(a + \varepsilon)$  with square flow area of dimension  $2a$  (Figure 2e). In Figure 6, the washcoat thickness  $\varepsilon$  has been varied from 0.05 in (a), 0.2 in (b), and 0.5 in (c). Similarly, Figure 7 shows the result for an equilateral triangular channel with inside triangle of dimension  $2a$  and center washcoat thickness of  $a\varepsilon$  (Figure 2h). Again, the results are shown for three different  $\varepsilon$  values of 0.05, 0.2, and 0.5, corresponding to Figures 7a, b, and c, respectively. Using the expressions for the effective transverse lengths given in Table 2, the parameter  $\lambda$  for the above channel geometries can be related to various channel dimensions as

$$\lambda = 2\varepsilon + \varepsilon_2 \quad \text{for square channel} \quad \text{and}$$

$$\lambda = 3\varepsilon^2 + 2\sqrt{3}\varepsilon \quad \text{for triangular channel}$$

As expected from the previous examples,  $Sh_{H_2,\infty}$  for triangular geometry (1.893) is lower than the  $Sh_{T,\infty}$  (2.497), whereas  $Sh_{H_2,\infty}$  for square geometry (3.089) is higher than the  $Sh_{T,\infty}$  (2.977). Also note that  $Sh_{H_1,\infty}$  is higher than  $Sh_{T,\infty}$  and  $Sh_{w,\infty}$  is lower than  $Sh_{H_2,\infty}$  (and hence  $Sh_{H_1,\infty}$ ) for both geometries. Hence, in the limit of  $\delta \rightarrow 0$ , the  $Sh_\infty$  decreases monotonically from  $Sh_{H_1,\infty}$  to  $Sh_{T,\infty}$  as catalyst loading is increased from 0 to  $\infty$ . It is now obvious that the washcoat profile does not have any direct influence in this regime except that the transition be-



**Figure 6. Asymptotic Sherwood number ( $Sh_\infty$ ) vs. surface Thiele modulus ( $\phi_s^2$ ) for a square channel with square flow area and with fully developed velocity profile.**

Results are shown for  $\delta$  values spanning the range of 0.001 to 500 for three different washcoat thicknesses of  $\varepsilon = 0.05$  in (a), 0.2 in (b), and 0.5 in (c).

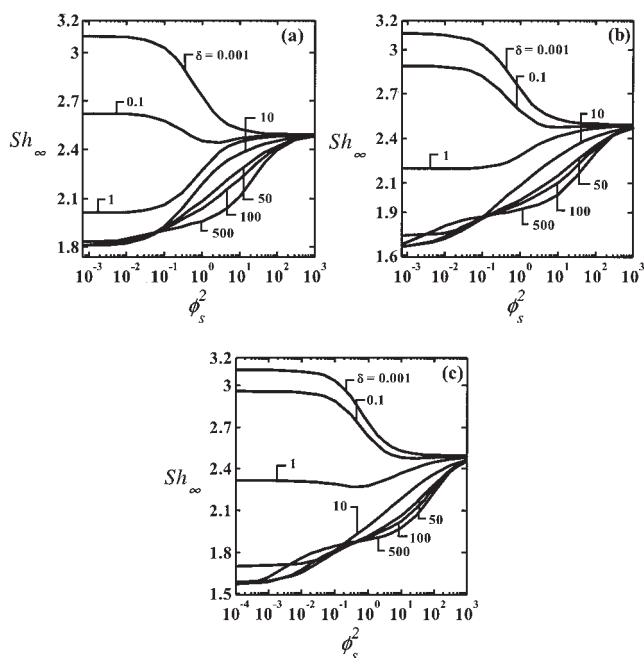


**Figure 7. Asymptotic Sherwood number ( $Sh_\infty$ ) vs. surface Thiele modulus ( $\phi_s^2$ ) for a triangular channel with triangular flow area and with fully developed velocity profile.**

Results are shown for  $\delta$  values spanning the range of 0.001 to 500 for three different washcoat thicknesses of  $\varepsilon = 0.05$  in (a), 0.2 in (b), and 0.5 in (c).

tween the asymptotes is a function of the washcoat properties. In the other limit of  $\delta \rightarrow \infty$ ,  $Sh_\infty$  starts with  $Sh_{w,\infty}$  of corresponding annular washcoat geometry at low catalyst loading of  $\phi_s^2 \rightarrow 0$  and reaches the  $Sh_{T,\infty}$  for high catalyst loading of  $\phi_s^2 \rightarrow \infty$ . In this limit,  $Sh_\infty$  increases monotonically with  $\phi_s^2$  for triangular geometry reaching  $Sh_{H_2,\infty}$  at  $\phi_s^2 \delta \lambda \sim 1$ . This creates a plateau around that point, as observed in the case of rounded triangular flow area with  $\sqrt{3} r/a < 0.4$ , whereas, for square geometry,  $Sh_\infty$  increases with catalyst loading ( $\phi_s^2$ ) until  $\phi_s^2 \delta \lambda \sim 1$ , where it reaches  $Sh_{H_2,\infty}$  which is higher than the constant temperature asymptote. Then,  $Sh_\infty$  decreases with further increases in  $\phi_s^2$  finally approaching  $Sh_{T,\infty}$  at  $\phi_s^2 \rightarrow \infty$ . This results in maxima in the  $Sh_\infty$  vs.  $\phi_s^2$  plots (as observed in earlier examples of rounded square geometry). As explained earlier, in all cases, the transition between various asymptotes depends on the washcoat properties and the transition zone consistently increases with increasing washcoat thickness. The hexagonal channel shows the same behavior as that of the square channel (results are not shown here).

## Discussion and Conclusions

We have determined the asymptotic mass-transfer coefficients in washcoated monoliths of various cross-sectional shapes by solving the convection–diffusion equation in the fluid phase coupled with the diffusion–reaction equation within the washcoat. Specifically, we have shown the effect of washcoat properties (such as geometry, relative effective washcoat thickness  $\lambda$ , relative washcoat diffusivity  $\delta$ , and catalyst loading  $\phi_s^2$ ) on the asymptotic mass-transfer coefficient or Sher-

wood number ( $Sh_\infty$ ). It is found that, in the kinetic regime ( $\phi_s^2 \ll 1$ ),  $Sh_\infty$  reaches a new asymptote  $Sh_{w,\infty}$  for  $\delta \gg 1$  with  $\phi_s^2 \delta \lambda \sim 1$ , which has not been reported in the literature.  $Sh_{w,\infty}$  is always found to be lower than the constant flux asymptotes and depends strongly on the washcoat geometry. It has also been observed that  $Sh_{w,\infty}$  approaches  $Sh_{H_1,\infty}$  (of flow geometry) in the limit of no washcoat diffusion ( $\delta \rightarrow 0$ ) and  $Sh_{H_2,\infty}$  (flow geometry) in the limit of strong washcoat diffusion ( $\delta \gg 1$  and  $\phi_s^2 \delta \lambda \gg 1$ ). On the other hand,  $Sh_\infty$  in the mass-transfer controlled regime ( $\phi_s^2 \gg 1$ ) is independent of the washcoat properties and reaches the constant concentration asymptote ( $Sh_{T,\infty}$ ) of the flow geometry for all  $\delta$  and  $\lambda$ . For channels with circular flow area,  $Sh_{H_1,\infty} = Sh_{H_2,\infty} = Sh_{w,\infty}$  and the dependency of asymptotic Sherwood number on washcoat properties in the kinetic regime vanishes, leading to the insensitivity of  $Sh_\infty$  in both kinetic and mass-transfer controlled regimes. It has also been shown that the transition from constant flux to constant concentration asymptote with increasing catalyst loading, which is not always monotonic, depends on the washcoat properties and is delayed to a higher  $\phi_s^2$  for thicker or denser washcoat.

It may be noted that, the exit cup-mixing concentration for first-order reaction can be obtained analytically from Eq. 19 as

$$c_{m,\text{exit}} = \sum_{n=1}^{\infty} \beta_n \exp\left(-\frac{\mu_n}{P}\right) \langle \Psi_1, 1 \rangle = \alpha_1 \exp\left(-\frac{\mu_1}{P}\right) \quad \text{for } P \ll 1 \quad (37)$$

where the first normalized Fourier constant  $\alpha_1$  is given by

$$\alpha_1 = \beta_1 \langle \Psi_1, 1 \rangle \quad (38)$$

whereas integration of the two-phase model results in the following expression for the exit cup-mixing concentration

$$c_{m,\text{exit}} = \exp\left(-\frac{\phi_s^2 \eta}{1 + \frac{4\phi_s^2 \eta P}{Sh_\infty}}\right) \quad (39)$$

which can be simplified for mass-transfer controlled regime as

$$c_{m,\text{exit}} = \exp\left(-\frac{Sh_{T,\infty}}{4P}\right) \quad (40)$$

It can be shown by algebraic manipulation that  $Sh_{T,\infty} = 4\mu_1$ . Note that the exit cup-mixing concentration predicted by the two-phase model differs from the analytical solution by the preexponential factor  $\alpha_1$ . This discrepancy can be attributed to the error in the initial condition used in the two-phase model. When the initial or inlet condition is modified to  $c_1 = \alpha_1$  at  $z = 0$ , the solution predicted by the two-phase model matches with the truncated one-term analytical expression. However, the variation of  $\alpha_1$  with  $\phi_s^2$  is much lower than the variation of  $Sh_\infty$  as shown in the sixth column of Table 1, which lists the values of  $\alpha_1$  for various channel geometries in the mass transfer controlled regime ( $\alpha_{1,T}$ ). Also,  $Sh_\infty$  appears in the exponential term. Thus, use of improper value for  $Sh_\infty$  will introduce a

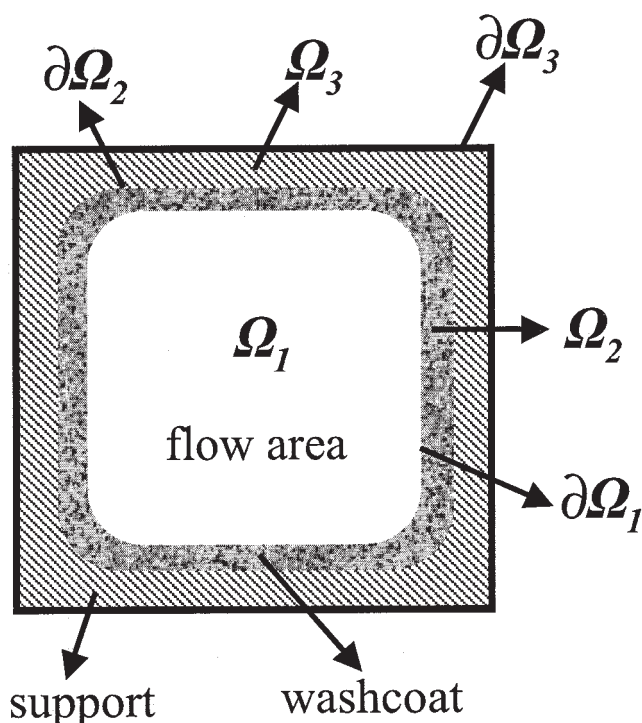


**Figure 8. Diagram illustrating different domains and heat-transfer resistances encountered in nonisothermal monolith channel.**

larger error in the cup-mixing concentration than  $\alpha_1$ , which is approximately 1 in the kinetic regime and about 0.8 in the mass transfer controlled regime.

To extend the above analysis to the nonisothermal monolithic channel, we have to consider the heat transfer through the support, which is impermeable to mass transfer, along with washcoat and fluid phase, as shown in Figure 8. The support is usually made of either ceramic (with low thermal conductivity) or metallic (with high thermal conductivity) material, which results in a wide variation of heat-transfer characteristics within the support, occurring mainly by conduction. For example, lower thermal conductivities of ceramic materials result in sharper temperature variations within the ceramic supports compared to those within the metallic ones. Similarly, the temperature profile within the washcoat depends mainly on the effective thermal conductivity of the washcoat and the heat of reaction. Consequently, the asymptotic Nusselt number ( $Nu_\infty$ ) in the kinetic regime, which depends on the ratios of thermal conductivities of solid phases (that is, support and washcoat) to that of the fluid phase, may reach different values depending on the combined heat-transfer resistance offered by support and washcoat. For example, in metallic supports and washcoat with high effective thermal conductivity,  $\delta \rightarrow 0$  and  $Nu_\infty$  attains the constant flux asymptote of the first kind ( $Nu_{H_1,\infty}$ ) of the flow geometry and is independent of the washcoat and support geometries. On the other hand, for ceramic supports and washcoat with low thermal conductivity,  $Nu_\infty$  may reach either  $Nu_{w,\infty}$  (for  $\phi_s^2 \rightarrow 0$  and  $\phi_s^2 \delta \lambda \sim 1$ ), which depends on the geometries and relative thicknesses of support, washcoat, and flow area or  $Nu_{H_2,\infty}$  of flow geometry (for  $\phi_s^2 \rightarrow 0$  and  $\phi_s^2 \delta \lambda \gg 1$ ), depending on the relative magnitude of  $\delta's$ .

Therefore, in the kinetic control regime ( $\phi_s^2 \rightarrow 0$ ), the asymptotic Nusselt number may reach values different from the asymptotic Sherwood number, depending on the support and washcoat materials. Nevertheless, in the mass transfer controlled regime,  $Nu_\infty$  reaches the constant temperature asymptote of the flow geometry as the asymptotic Sherwood number. It should be pointed that the accurate values for the asymptotic Sherwood or Nusselt numbers in the kinetic regime are needed to predict the light-off or ignition point accurately, as shown by Gupta and Balakotaiah (2001).

Finally for irregular geometries such as those shown in Figure 1c (which are observed in many natural systems such as oxygen transport through blood vessels), the calculated Sherwood number might be lower than that in regular geometries. For example,  $Sh_\infty$  calculated for a domain with more than one circular flow area of different radius, is lower than that obtained for one circle with the same total flow area. However, the interfacial area increases with increasing number of circles keeping the total flow area the same, and the increase in interfacial area is much more than the decrease in  $Sh_\infty$  and increases the total mass transfer through the solid-fluid interface. Similarly, for the case of mass transfer of reacting species across a gas bubble surrounded by liquid layer with homogeneous reaction as in a gas-liquid reactor, the mass transfer coefficients depend on the geometric shapes and hold-up of gas bubble and surrounding liquid layer, which can be calculated by following a formulation that is similar to that presented in this work.

## Acknowledgments

This work was supported by the Texas Advanced Technology program. The work of V. Balakotaiah was also supported by the Robert A. Welch Foundation and the Dow Chemical Company.

## Notation

- $a$  = transverse dimension of washcoated channel
- $a_v$  = solid-fluid interfacial area per unit volume
- $A_{\Omega_1}$  ( $A_{\Omega_2}$ ) = cross-sectional area of fluid phase (washcoat)
- $c_1$  ( $c_2$ ) = dimensionless reactant concentration in fluid (solid) phase
- $c_m$  ( $c_s$ ) = dimensionless cup-mixing (averaged interfacial) concentration
- $D_m$  = molecular diffusivity of the reactant in the fluid phase
- $D_e$  = effective diffusivity of the reactant within washcoat
- $d_h$  = channel hydraulic diameter
- $Da$  = Damköhler number
- $Da_{loc}$  = local Damköhler number or the surface Thiele modulus
- $f(x', y')$  = local fluid-phase velocity profile
- $g(x, y)$  = dimensionless local fluid-phase velocity profile
- $k_c$  = mass transfer coefficient from the bulk of the fluid to the substrate
- $k_v$  = first-order rate constant based on unit washcoat volume
- $L$  = length of the channel
- $Nu_\infty$  = asymptotic Nusselt number
- $P$  = transverse Peclet number
- $P_\Omega$  ( $P_{\Omega_w}$ ) = wetted (fluid-solid interfacial) perimeter
- $R$  = radius of the circular flow area
- $r$  = radius of the rounded corner
- $R_{\Omega_1}$  ( $R_{\Omega_2}$ ) = effective transverse diffusion length for flow (washcoat) area
- $Sc$  = Schmidt number
- $Sh$  ( $Sh_\infty$ ) = Sherwood (asymptotic) number
- $\langle u \rangle$  = average fluid velocity
- $x, y$  = dimensionless transverse coordinate
- $z$  = dimensionless axial coordinate

## Greek letters

- $\varepsilon$  = dimensionless washcoat thickness  
 $\alpha$  = aspect ratio  
 $\delta$  = ratio of reactant diffusivities in the fluid phase and the washcoat  
 $\delta\Omega_f (\delta\Omega_2)$  = dimensionless solid–fluid interfacial (outer channel wall) boundary  
 $\lambda$  = ratio of transverse diffusion lengths of washcoat to fluid phase  
 $\mu_n$  =  $n$ th eigenvalue  
 $\eta$  = effectiveness factor  
 $\Omega_f (\Omega_2)$  = dimensionless cross-sectional domain of fluid phase (washcoat)  
 $\xi$  = dimensionless transverse coordinate for circular channel  
 $\phi_s^2$  = surface Thiele modulus or local Damköhler number  
 $\phi_s^2$  = washcoat Thiele modulus  
 $\Phi_s^2$  = modified Thiele modulus  
 $\Psi_{f,n} (\Psi_{2,n} \Psi_n)$  =  $n$ th eigenfunction in domain  $\Omega_1 (\Omega_2, \Omega_1 \cup \Omega_2)$

## Literature Cited

- Ablow, C. M., and H. Wise, "Theoretical Analysis of Catalytic Combustion in a Monolith Reactor," *Combust. Sci. Technol.*, **21**, 35 (1979).  
 Aris, R., *The Mathematical Theory of Diffusion and Reaction in Permeable Catalysts*, Vol. 1, Clarendon Press, Oxford, UK (1975).  
 Balakotaiah, V., N. Gupta, and D. H. West, "A Simplified Model for Analyzing Catalytic Reactions in Short Monoliths," *Chem. Eng. Sci.*, **55**, 5367 (2000).  
 Bennett, C. J., R. E. Hayes, S. T. Kolaczkowski, and W. J. Thomas, "An Experimental and Theoretical Study of a Catalytic Monolith to Control Automobile Exhaust Emissions," *Proc. R. Soc. London Ser. A Math. Phys. Eng. Sci.*, **439**, 465 (1992).  
 Bennett, C. J., S. T. Kolaczkowski, and W. J. Thomas, "Determination of Heterogeneous Reaction-Kinetics and Reaction-Rates under Mass-Transfer Controlled Conditions for a Monolith Reactor," *Process Safety Environ. Protection*, **69**, 209 (1991).  
 Bensalem, O., and W. R. Ernst, "Mathematical Modeling of Homogeneous–Heterogeneous Reactions in Monolithic Catalysts," *Combust. Sci. Technol.*, **29**, 1 (1982).  
 Cybulski, A., and J. A. Moulijn, "Monoliths in Heterogeneous Catalysis," *Catal. Rev. Sci. Eng.*, **36**, 179 (1994).  
 Damköhler, G., "Influence of Diffusion, Fluid Flow and Heat Transport on the Yield in Chemical Reactor," *Chem.-Ing.-Tech.*, **3**, 359 (1937).  
 Forzatti, P., "Present Status and Perspectives in de-NO<sub>x</sub> SCR Analysis," *Appl. Catal. A General*, **222**, 221 (2001).  
 Gropi, G., and E. Tronconi, "Theoretical Analysis of Mass and Heat Transfer in Monolith Catalysts with Triangular Channels," *Chem. Eng. Sci.*, **52**, 3521 (1997).  
 Gupta, N., and V. Balakotaiah, "Heat and Mass Transfer Coefficients in Catalytic Monoliths," *Chem. Eng. Sci.*, **56**, 4771 (2001).  
 Hayes, R. E., and S. T. Kolaczkowski, "Mass and Heat-Transfer Effects in Catalytic Monolith Reactors," *Chem. Eng. Sci.*, **49**, 3587 (1994).  
 Hayes, R. E., S. T. Kolaczkowski, and W. J. Thomas, "Finite Element Model for a Catalytic Monolith Reactor," *Comput. Chem. Eng.*, **16**, 645 (1992).  
 Heck, R. H., J. Wei, and J. R. Katzer, "Mathematical Modeling of Monolithic Catalysts," *AIChE J.*, **22**, 477 (1976).  
 Hegedus, L. L., "Temperature Excursions in Catalytic Monoliths," *AIChE J.*, **21**, 849 (1975).  
 Lee, A., and R. Aris, "On the Effects of Radiative Heat Transfer in Monoliths," *Chem. Eng. Sci.*, **32**, 827 (1977).  
 Leung, D., R. E. Hayes, and S. T. Kolaczkowski, "Diffusion Limitation Effects in the Washcoat of a Catalytic Monolith Reactor," *Can. J. Chem. Eng.*, **74**, 94 (1996).  
 Oh, S. H., and J. C. Cavendish, "Design Aspects of Poison-Resistant Automobile Monolith Catalyst," *Ind. Eng. Chem. Prod. Res. Dev.*, **22**, 509 (1983).  
 Papadakis, D., L. Edsberg, and P. Björnborn, "Simplified Method for Effectiveness Factor Calculations in Irregular Geometries of Washcoats," *Chem. Eng. Sci.*, **55**, 1447 (2000).  
 Shah, R. K., and A. L. London, "Laminar Flow Forced Convection in Ducts," *Advances in Heat Transfer (Suppl. 1)*, Academic Press, New York (1978).  
 Tronconi, E., and P. Forzatti, "Adequacy of Lumped Parameter Models for SCR Reactors with Monolith Structure," *AIChE J.*, **38**, 201 (1992).  
 Ullah, U., S. P. Waldram, C. J. Bennett, and T. Truex, "Monolithic Reactors: Mass Transfer Measurements under Reacting Conditions," *Chem. Eng. Sci.*, **47**, 2413 (1992).  
 Votruba, J., O. Mikuš, N. Khue, V. Hlaváček, and J. Skřivánek, "Heat and Mass Transfer in Honeycomb Catalysts—II," *Chem. Eng. Sci.*, **30**, 201 (1975).  
 Young, L. C., and B. A. Finlayson, "Mathematical Models of the Monolith Catalytic Converter: I," *AIChE J.*, **22**, 331 (1976a).  
 Young, L. C., and B. A. Finlayson, "Mathematical Models of the Monolith Catalytic Converter: II," *AIChE J.*, **22**, 343 (1976b).

Manuscript received Dec. 1, 2003, and revision received Feb. 13, 2004.